AD_____
(Leave blank)

Award Number: W81XWH-06-1-0221

TITLE:
Role of Merlin in the Growth and Transformation of Arachnoidal Cells

PRINCIPAL INVESTIGATOR:
Anita Lal, Ph.D.

CONTRACTING ORGANIZATION: Regents of the University of California
San Francisco, CA 94143-0962

REPORT DATE:
January 2009

TYPE OF REPORT:
Annual

PREPARED FOR: U.S. Army Medical Research and Materiel Command
Fort Detrick, Maryland 21702-5012

DISTRIBUTION STATEMENT: (Check one)

X Approved for public release; distribution unlimited

☐ Distribution limited to U.S. Government agencies only; report contains proprietary information

The views, opinions and/or findings contained in this report are those of the author(s) and should not be construed as an official Department of the Army position, policy or decision unless so designated by other documentation.

REPORT DOCUMENTATION PAGE

Form Approved
OMB No. 0704-0188

1. REPORT DATE *(DD-MM-YYYY)*	**2. REPORT TYPE**	**3. DATES COVERED** *(From - To)*
27-01-2009	Annual	28 DEC 2007 - 27 DEC 2008

4. TITLE AND SUBTITLE
Role of Merlin in the Growth and Transformation of Arachnoidal *
Cells

5a. CONTRACT NUMBER
W81XWH-06-1-0221

5b. GRANT NUMBER
NF050061

5c. PROGRAM ELEMENT NUMBER

6. AUTHOR(S)
Anita Lal;

5d. PROJECT NUMBER

5e. TASK NUMBER

5f. WORK UNIT NUMBER

7. PERFORMING ORGANIZATION NAME(S) AND ADDRESS(ES)

Regents of the University of California
c/o Office of Sponsored Research
3333 California Street, Ste. 315
San Francisco, CA 94143-0962 (use 94118 for overnight mail)

8. PERFORMING ORGANIZATION REPORT NUMBER

9. SPONSORING / MONITORING AGENCY NAME(S) AND ADDRESS(ES)
U.S. Army Medical Research and Materiel Command
Fort Detrick, Maryland 21702-5012

10. SPONSOR/MONITOR'S ACRONYM(S)

11. SPONSOR/MONITOR'S REPORT NUMBER(S)

12. DISTRIBUTION / AVAILABILITY STATEMENT

Approved for public release; distribution unlimited

13. SUPPLEMENTARY NOTES

14. ABSTRACT
This proposal is concerned with the functional role of merlin in arachnoidal and meningioma cells. In year 1, we developed meningioma-specific NF2 model systems. In Year 2, we characterized the phenotypic effects of these model systems. We showed that merlin loss enhances loss of contact inhibition of growth, increases anchorage independent growth and increases S-phase entry. In the final year, we have shown that merlin loss promotes tumor growth in athymic mice and have developed *in vivo* xenograft models of NF2 that can be monitored non-invasively using bioluminescent imaging using the *in vitro* matched cell lines. We have completed a microarray analysis of our matched NF2 cell lines, and have identified several potential downstream targets of merlin loss in meningiomas. Several of these are cell cycle and apoptosis-related proteins and members of other signaling pathways suggesting cross talk between merlin and these pathways.

15. SUBJECT TERMS
Merlin, meningioma, arachnoidal cells, RNA interference, Retroviral mediated gene transfer, flow cytometry,

16. SECURITY CLASSIFICATION OF:			**17. LIMITATION OF ABSTRACT**	**18. NUMBER OF PAGES**	**19a. NAME OF RESPONSIBLE PERSON**
a. REPORT	**b. ABSTRACT**	**c. THIS PAGE**			USAMRMC
U	U	U	UU	40	**19b. TELEPHONE NUMBER** *(include area code)*

Table of Contents

LAL, ANITA

INTRODUCTION

Neurofibromatosis 2 (NF2) is a cancer predisposition syndrome that is phenotypically characterized by the presence of multiple benign brain tumors, primarily schwannomas and meningiomas. Intracranial meningiomas, often multicentric, occur in ~50% of NF2 patients and are associated with an increased risk of mortality. The majority of studies evaluating the mechanism of action of the NF2 gene product, merlin, have used cell lines unrelated to NF2 target cells. Since tumor suppressor function is cell-type specific, the relevance of these studies to the function of merlin in meningiomas is unclear. Additionally, conditional NF2 mouse modeling studies and genotype-phenotype correlation studies suggest mechanistic differences in the function of NF2 between schwannomas and meningiomas. The purpose of this study is to develop meningioma-specific NF2 model systems and to use these model systems to investigate the specific tumor suppressive function of NF2 in meningioma development. Our strategy is to isolate and immortalize human meningioma and arachnoidal cell lines, characterize the expression of merlin in these *in vitro* systems and to engineer merlin-deficient or merlin-expressing meningioma and arachnoidal cells in the relevant genetic backgrounds. These NF2 model systems will be used to dissect the pathways and mechanisms by which merlin expresses its growth suppressive effects specifically in meningioma tumorigenesis.

BODY

Outlined below is a summary of the research accomplishments associated with each task outlined in the approved Statement of Work. Tables and Figures related to the text are included in the Supporting Data Section. Appendix 1 includes three publications from my laboratory. The first manuscript, (1), is a direct result of this funding. The other two manuscript, (2, 3), contain results and procedures that are pertinent to this report. We refer to Appendix 1 when referring to a figure in these manuscripts. For example, (Figure 1 in Manuscript 1, Appendix 1) would imply Figure 1 in the first attached manuscript in Appendix 1, (Figure 2 in Manuscript 3, Appendix 1) would imply Figure 2 in the third attached manuscript in Appendix 1, while (Figure 1) refers to the Supporting Data Section.

Task 1. Characterize merlin expression in immortalized meningioma cell lines (Months 1- 24).

a. *Three additional immortalized meningioma cell lines will be generated using telomerase alone or in conjunction with the human papillomavirus E6/E7 oncogene (Months 1-6).*

This task was described in detail in the Year 1 Annual Report. Briefly, we generated a total of nine meningioma and three arachnoidal cell lines in my laboratory. The strategy used to generate these cell lines is described in detail in Manuscript 2, Appendix 1.

b. Merlin-deficient cell lines will be chosen using western blot analysis (Months 4-7).

This task was described in detail in the Year 1 Annual Report. Briefly, KT21MG1 was identified as a merlin deficient meningioma cell line, and SF6717 was identified as a merlin positive meningioma cell line. SF6717 is a new cell line established in our laboratory that has been renamed MENII-1 to reflect the fact that it is a meningioma cell line derived from a WHO Grade II tumor. In the rest of this report, we refer to this cell line as MENII-1. Arachnoidal cells (AC1) were merlin positive.

c. Vector-control and merlin-expressing stable clones will be generated in appropriate meningioma cell lines (Months 6-12).

d. The expression of merlin will be assessed in individual stable clones and clones expressing high levels of merlin will be chosen (Months 11-14).

These tasks were described in detail in the Year 1 Annual Report. Briefly, we expressed wild-type NF2 and three specific mutants of merlin (L64P, S518A and S518D) in the KT21MG1 cell line. We show the expression of merlin in KT21MG1-NF2 cells by western blot analysis and immunofluorescence (Figure 2 in Manuscript 1, Appendix 1).

e. *Functional in vitro assays for cell proliferation, apoptosis, motility/invasion and survival will be performed (Months 15-24).*

The experiments performed for this task were described in the Year 2 Annual Report and are briefly summarized with Task 2d below.

Task 2. Establish an in vitro model of merlin loss in human arachnoidal cells and evaluate the consequent changes in cell growth, motility and survival (Months 1-36).

a. *Chemically synthesized siRNA for merlin will be obtained and the efficacy of these siRNA to downregulate merlin will be tested using transient transfections (Months 1-6).*
b. *Merlin-specific siRNA plasmid will be constructed and stable clones expressing merlin siRNA will be generated in immortalized arachnoidal cells (Months 7-11).*
c. *The extent of downregulation of merlin will be evaluated in individual stable clones and the clone with the greatest level of knockdown of merlin will be chosen (Months 12-14).*

These tasks were described in detail in the Year 1 and Year 2 Annual Report. Briefly, we chose NF2siRNA3 to achieve stable suppression of NF2 in arachnoidal (AC1) and MENII-1 meningioma cell lines. Stable cell populations expressing either NF2 siRNA (MENII-1-NF2 siRNA or AC1-NF2 siRNA) or a non-specific target siRNA (MENII-1-Control or AC1-Control) were generated. NF2 transcript and protein levels were considerably lower in MENII-1-NF2 siRNA and AC1-NF2 siRNA compared to MENII-1-Control and AC1-Control respectively (Figure 2 in Manuscript1, Appendix 1). NF2 siRNA was effective at stably suppressing the expression of endogenous merlin.

d. *Functional in vitro assays for cell proliferation, apoptosis, motility/invasion and survival will be performed on the merlin deficient arachnoidal cells (Months 15-24).*

These tasks were described in detail in the Year 2 Annual Report. Briefly, we showed that NF2 loss resulted in loss of contact dependent inhibition of growth and promoted colony formation in soft agar (Figure 3 in Manuscript1, Appendix1). This is consistent with previous results suggesting that merlin has a direct effect on loss of contact dependent inhibition of growth (4). We also showed that merlin loss resulted in a pronounced increase in the number of cells in the S-phase (Figure 4 in Manuscript1, Appendix1). Thus, merlin was affecting the G0-G1 to S phase cell cycle checkpoint in meningioms. Finally, we showed that merlin loss resulted in increased Cyclin E1 protein levels (Figure 6 in Manuscript1, Appendix1). Cyclin E1 regulates G0-G1 to S transition (5, 6) and it is likely that merlin regulates G0-G1 to S phase transition by affecting Cyclin E1 levels. Consistent results were obtained in all three meningioma and arachnoidal cell lines and using two independent means of manipulating merlin levels (retroviral mediated gene transfer and RNA interference).

e. *The in vivo ability of these cell lines to form tumors will be tested and the resultant tumors will be characterized (Months 27-36*).

In Year 3, we have assessed the ability of the AC1-Control, AC1-NF2 siRNA, MENII-I-Control, MENII-1-NF2 siRNA, KT21MG1-Control and KT21MG1-NF2 to form tumors in athymic mice. The strategy used to implant these cells in the skull base region of athymic mice is described in detail in Manuscript 3, Appendix 1. Briefly, these cells are resuspended in matrigel and implanted using a stereotactic apparatus at co-ordinates: 2 mm to the right of the bregma, 2 mm posterior to the bregma and 5.8 mm below the skull surface. Intracranial growth of these cell lines was non-invasively monitored using bioluminescence. In order to be able to monitor these cell lines using bioluminescence, they were infected with a luciferase containing lentivirus as described in Manuscript 2, Appendix1. AC1-Control and MENII-I-Control cells were non-tumorigenic in mice and did not produce tumors. However, stable suppression of NF2 expression in these cell lines resulted in the growth of aggressive tumors that could be monitored by bioluminescence (Figure 1). In both cases, the luminescent signal was strong by day 10 and increased exponentially. Bioluminescent signal has been shown to be directly correlated with tumor size, suggesting that tumors in these mice were growing at a rapid rate. While AC1-Control and MENII-1-Control mice continued to remain healthy and tumor-free till Day 50, AC1-NF2

siRNA and MENII-1-NF2 siRNA mice had estimated survival times of 15-18 days (Figure 2). Macroscopic examination of the skull base regions of these mice revealed large tumor masses that was localized between the skull and the brain and did not invade the surface of the brain, similar to human meningiomas. We are currently examining the detailed histopathological characteristics of these tumors (using no-cost extension funding).

In the KT21MG1, a malignant meningioma cell line, both control and NF2 expressing KT21MG1 cells formed tumors. However, merlin expression slowed tumor growth (Figure 3A). Estimated survival times for KT21MG1-NF2 was significantly longer went compared to KT21MG1-Control cells (Figure 3B). Tumor masses between the skull and the brain was once again observed. However, a greater degree of leptomeningeal dissemination was observed in the KT21MG1 tumor model. There was great variability in the survival times of these mice ranging from 4 weeks to 18 weeks. We have thus obtained three different NF2 deficient xenograft models in athymic mice, and these models are expected to be very useful as preclinical models of neurofibromatosis 2 for testing the efficacy of therapeutic agents.

Task 3. Identify and characterize downstream target genes that are regulated by merlin in meningioma and arachnoidal cells (Months 18-36).

a. *Two SAGE libraries will be constructed and sequenced from the vector-control and merlin-deficient arachnoidal cells (Months 18-21).*
b. *Two SAGE libraries will be constructed and sequenced from the vector-control and merlin-expressing meningioma cells (Months 21-25).*
c. *Bioinformatics will be performed to analyze the SAGE data and to functionally classify differentially expressed genes (Months 26-29).*

In the Year 2 annual report, we described our rationale for performing microarray analysis instead of SAGE analysis. Microarray is a technology comparable to SAGE, and analyzes the transcriptomes of cell lines or tumors. Since microarray is more cost-effective, it allowed us to compare the transciptomes of AC1-Control and MENII-1-Control cell lines to that of the AC1-NF2 siRNA and MENII-1-NF2 siRNA cell lines respectively. Microarray analysis was performed in triplicates in these four stable cell lines. The data was analyzed similar to procedures described in (7). Genes that were differentially expressed between the merlin-positive and merlin-negative cell lines were identified independently for AC1 and MENII-1. Twenty three genes, listed in Table 1, were in common between AC1 and MENII-1.

d. *Quantitative PCR analysis will be initiated on select target genes affected by merlin* (Months 30-36).

We are currently completing the Quantitative PCR analysis of select target genes of merlin identified by the microarray analysis. This will be completed in the No Cost Extension Period.

In summary, we have successfully completed the majority of proposed tasks for this three-year proposal. The tumors took longer to grow than anticipate and we had technical difficulties with the quantitative PCR machine. We anticipate completion of the animal work including characterization of the tumors, and completion of the quantitative PCR work in the No Cost Extension period.

KEY RESEARCH ACCOMPLISHMENTS

1) We have successfully generated and characterized paired human meningioma cell lines where the only difference is expression of merlin using either RNA interference or retroviral mediated gene transfer.
2) We have used these paired cell lines to show that absence of merlin causes loss of contact inhibition of growth,enhanced anchorage independent growth in soft agar and an increase in S-phase entry.
3) We have shown that merlin loss is associated with an increase in transcript and protein levels of cyclin E1.
4) Merlin loss has an effect on the apoptotic rates in meningioma cell lines. Merlin loss causes a decrease in spontaneous apoptotic rates and also increases resistance to Stsp-mediated apopotosis.
5) Using the paired cell lines described above, we have generated three *in vivo* xenograft models in athymic mice.
6) We have completed a Microarray analysis on the paired cell lines and have identified a list of downstream target genes that are affected by merlin expression.

REPORTABLE OUTCOMES

1) We have also generated three sets of paired meningioma cell lines where the only difference is the expression of merlin. These are KT21MG1-Control and KT21MG1-NF2; AC1-Control and AC1-NF2 siRNA; and MENII-1-Control and MENII-1-NF2 siRNA.
2) We have characterized, in great detail, the phenotypic effects of merlin loss on these cell lines
3) We have developed meningioma-specific *in vivo* Neurofibromatosis 2 model systems.
4) Using results of this research we obtained a concept award from the DOD neurofibromatosis program. The results of the concept award identified the Hippo Signaling Pathway as downstream of Merlin, and have worked out the details of this signaling mechanism.
5) We have successfully published a research publication in Neoplasia using the data described in this proposal. In addition, we have another research publication that will be submitted within the next two months for peer review.

CONCLUSION

The aim of this proposal is to develop meningioma-specific NF2 model systems and to utilize these systems to investigate the tumor suppressive functions of NF2 in meningiomas. Year 1 of this proposal was focused on characterizing and generating the relevant model systems. Year 2 of this proposal was focused on characterizing the phenotypic effects of these cell lines. In Year 3, we developed *in vivo* models of Neurofibromatosis 2 in athymic mice and identified downstream targets of merlin loss in meningiomas. In a complimentary study funded by a concept award from the DOD, we have also identified that Merlin signals through the Hippo Pathway to regulate cell growth. Altogether, this work has resulted in *in vitro* and *in vivo* tools to be able to study meningioma formation in neurofibromatosis 2, an understanding of the phenotypic effects of merlin loss in meningiomas, a genetic model of meningiomas, and an understanding of the signaling mechanism(s) that merlin uses to exert its tumor suppressive effects. We expect that the in vivo models will be used as a preclinical tool to assess the efficacy of novel therapeutic agents for neurofibromatosis 2.

REFERENCES

1. Striedinger K, VandenBerg SR, Baia GS, McDermott MW, Gutmann DH, Lal A. The neurofibromatosis 2 tumor suppressor gene product, merlin, regulates human meningioma cell growth by signaling through YAP. Neoplasia 2008;10(11):1204-12.
2. Baia GS, Slocum AL, Hyer JD, *et al.* A genetic strategy to overcome the senescence of primary meningioma cell cultures. J Neurooncol 2006;78(2):113-21.
3. Baia GS, Dinca EB, Ozawa T, *et al.* An orthotopic skull base model of malignant meningioma. Brain Pathol 2008;18(2):172-9.
4. Morrison H, Sherman LS, Legg J, *et al.* The NF2 tumor suppressor gene product, merlin, mediates contact inhibition of growth through interactions with CD44. Genes Dev 2001;15(8):968-80.
5. Bartek J, Lukas J. Pathways governing G1/S transition and their response to DNA damage. FEBS Lett 2001;490(3):117-22.
6. Porter DC, Zhang N, Danes C, *et al.* Tumor-specific proteolytic processing of cyclin E generates hyperactive lower-molecular-weight forms. Mol Cell Biol 2001;21(18):6254-69.
7. Carvalho LH, Smirnov I, Baia GS, *et al.* Molecular signatures define two main classes of meningiomas. Molecular cancer 2007;6(1):64.

BIBLIOGRAPHY

PUBLICATIONS

Striedinger KS, VandenBerg SR, Baia GS, McDermott MW, Gutmann DH and Lal A: The neurofibromatosis 2 tumor suppressor gene product, merlin, regulates meningioma cell growth by signaling through YAP. Neoplasia 10:1204-12, 2008

MEETING ABSTRACTS

6th International Congress on Meningioma and Cerebral Venous System, Boston, September 2008

The neurofibromatosis 2 gene product, merlin, regulates S-phase entry by signaling through YAP in meningiomas
Katherine Striedinger, Michael W McDermott, David H Gutmann, Scott R VandenBerg and Anita Lal

INTRODUCTION
Neurofibromatosis type-2 (NF2) is an autosomal dominant disorder characterized by the occurrence of multiple benign brain tumors, primarily schwannomas and meningiomas. The molecular mechanism(s) by which the NF2 gene product, merlin, acts as a tumor suppressor is unclear. In *Drosophila*, merlin controls cell proliferation and apoptosis by signaling through the Hippo pathway and its effector protein, the cotranscriptional activator *yorkie*. However, whether merlin acts through the Hippo pathway in human cells is unknown.
METHODS
To investigate the functional association between merlin and YAP, the human ortholog of *yorkie*, we have used RNA interference and retroviral mediated gene transfer to develop paired human meningioma cell lines where the only difference is merlin expression. We have evaluated YAP levels using western blots and immunofluorescence. Finally, we have used flow cytometry to assess S-phase entry.
RESULTS

Absence of merlin was associated with loss of contact dependent inhibition of growth, anchorage independent growth, increased S-phase entry and enhanced cyclin E expression. Protein levels of YAP was elevated and localized into the nucleus in NF2 negative meningioma cell lines. Sporadic meningioma tumors lacking merlin expression also had elevated levels of nuclear YAP. Moreover, depletion of YAP reversed the cell proliferation effects caused by merlin loss.
CONCLUSIONS
Collectively, our data shows that merlin exerts its tumor suppressor function, at least in part, by inducing YAP expression in meningioma tumors, and suggests a functional conservation of the hippo pathway effectors between *Drosophila* and humans.

Annual Meeting of the Society for Neuro-oncology, Dallas, November 2007

NF2 tumor suppressor function acts through the hippo pathway in human meningiomas
Katherine Striedinger, David H Gutmann, and Anita Lal

Neurofibromatosis type-2 (NF2) is a cancer predisposition syndrome caused by mutations in the NF2 gene, and is characterized by the occurrence of meningiomas. Thus loss of NF2 and its product merlin are critical for the development of meningiomas. In this study we explored the molecular mechanisms by which NF2 acts as a tumor suppressor in an immortalized human meningioma cell line (MEN II-1). NF2 expression was stably suppressed by RNA interference in MEN II-1. As expected, loss of contact dependent inhibition, anchor independent growth, and increased proliferation was observed when NF2 was silenced. The function of merlin as a negative regulator of growth is described in *Drosophila* where it has recently been shown to act upstream of the Hippo signalling pathway, regulating cell proliferation and apoptosis. We hypothesized that merlin could exert its tumor suppressor function through the mammalian homologue of the hippo pathway in humans. To test this hypothesis, we analyzed the function and expression of YAP, the mammalian homologue of the effector protein of the hippo pathway (Yorkie). We found that YAP was upregulated when NF2 was silenced. Interestingly, the increased proliferation documented in NF2 deficient cells was reversed to control levels by downregulation of YAP. These results show for the first time in meningioma human cells a functional relationship between NF2 tumor suppressor and YAP. Current research is conducted to understand how merlin signals YAP in humans.

PERSONNEL RECEIVING PAY FROM THIS RESEARCH EFFORT

Anita Lal, Ph.D.
Katherine Striedinger, MD, PhD
Gilson S Baia, MS

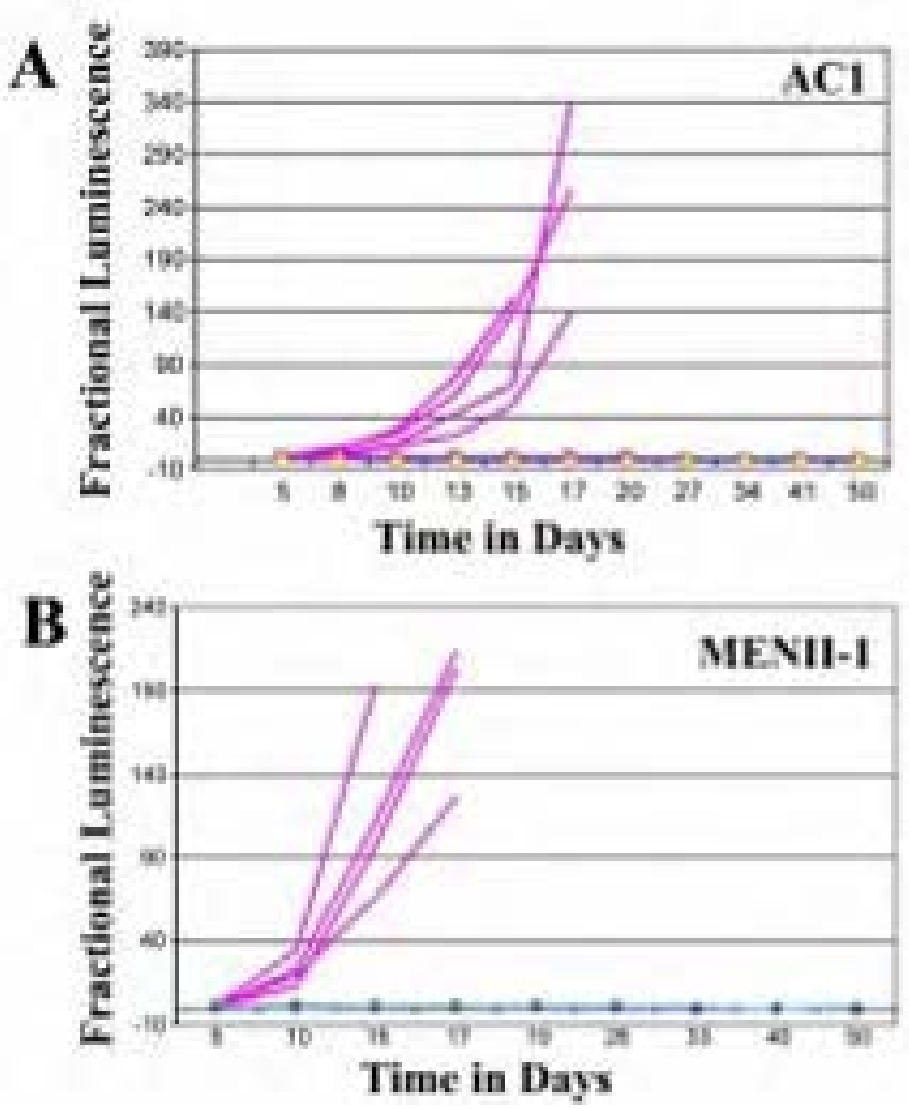

Figure 1. Bioluminescent (BLI) imaging of meningioma xenografts . Luminescence readings for each mouse (4 in each group as an example) were normalized against its own day 5 luminescence reading for AC1 (Panel A) and MENII-1 (Panel B). Normalized BLI plots associated with monitoring of intracranial tumor growth for control (Blue lines) and NF2 siRNA (Pink lines) groups are shown.

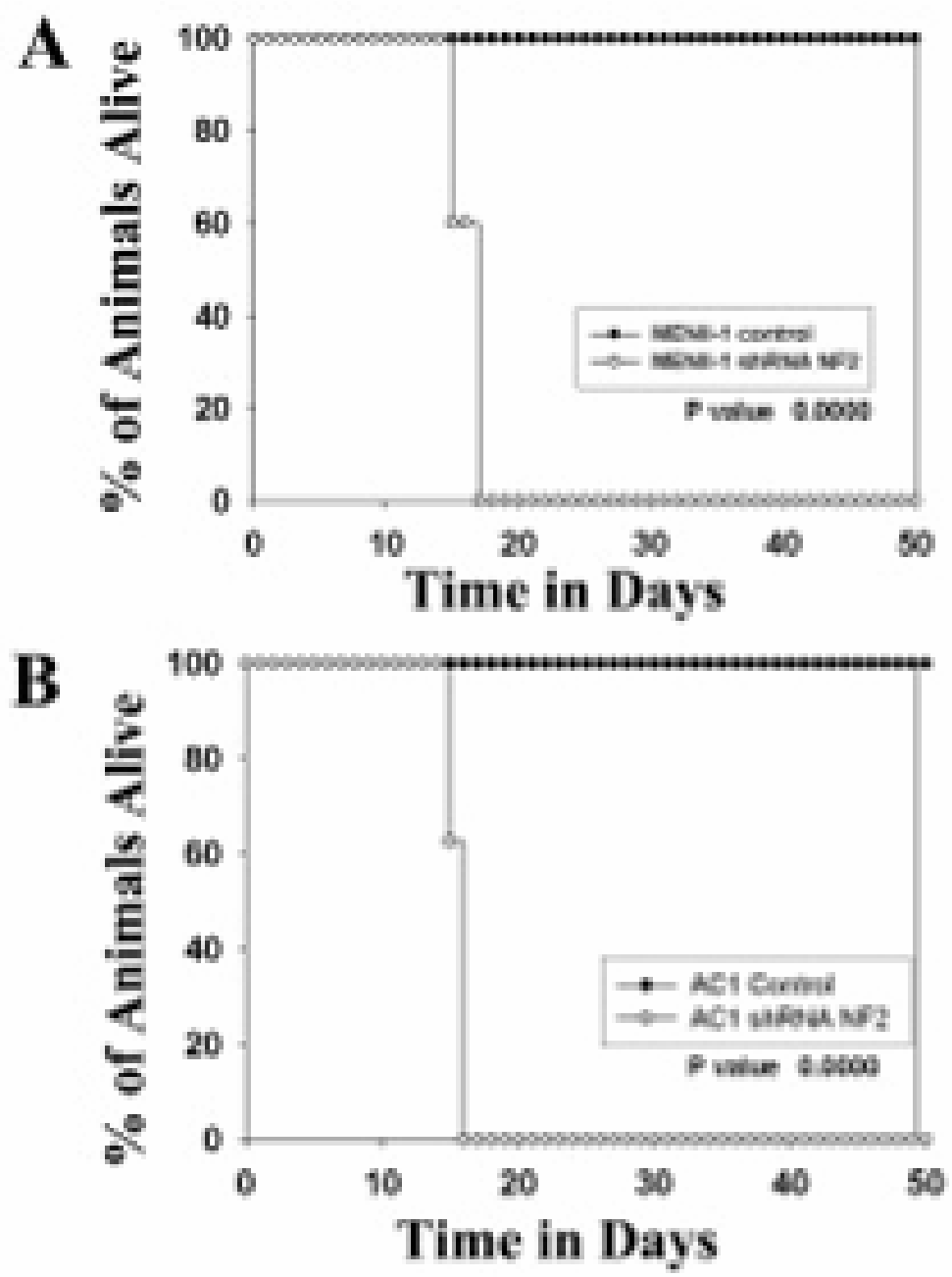

Figure 2. Estimated survival curves of athymic mice implanted with MEN II-1 (A) or AC1 (B) cells. Athymic mice implanted with 3 million cells/3 μL were euthanized when they exhibited neurological symptoms or weight loss. Mice implanted with cell lines with loss of merlin (MENII-I shRNA NF2 and AC1 shRNA NF2) had significantly lower survival times when compared to the mice implanted with the corresponding control cell lines (MENII-I Control and AC1 Control).

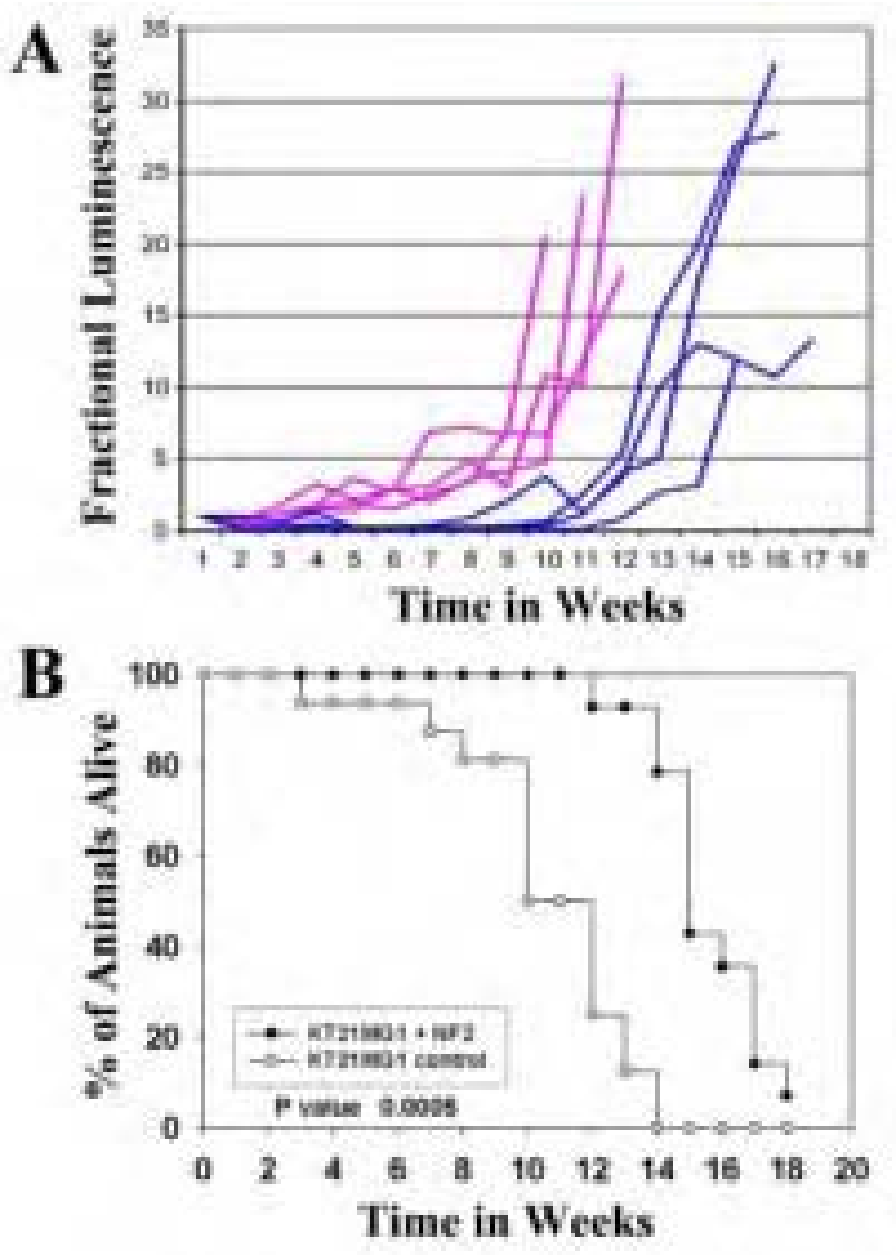

Figure 3. Bioluminescent (BLI) imaging and estimated survival times of athymic mice with KT21MG1 xenografts. **A)** Luminescence readings for each mouse (4 in each group as an example) were normalized against its own day 7 day luminescence reading for KT21MG1. Normalized BLI plots associated with monitoring intracranial tumor growth for control (Pink lines) and NF2 expressing (Blue lines) groups are shown. **B)** Mice implanted with KT21MG1-Control cells had significantly lower survival times when compared to KT21MG1-NF2 cells.

Table 1: Merlin Target Genes in Common Between AC1 and MENII-1

ID	Genes Altered in Both AC1 and MENII-1	Fold Change (AC1)	Fold Change (MENII-1)
1	BEX2 (84707) 23:102451 kb; protein-coding	0.0495	0.1444
2	DMKN (93099) 19:40680 kb; protein-coding	0.0531	0.1187
3	HEY1 (23462) 8:80839 kb; protein-coding	0.047	0.0897
4	LIN28B (389421) 6:105512 kb; protein-coding	0.0476	0.0524
5	MAGEA1 (4100) 23:152135 kb; protein-coding	0.0499	0.0748
6	CALCB (797) 11:15052 kb; protein-coding	0.0493	0.0805
7	RNF128 (79589) 23:105824 kb; protein-coding	0.0488	0.0664
8	HS6ST2 (90161) 23:131588 kb; protein-coding	0.0737	0.09
9	SLAIN1 (122060) 13:77170 kb; protein-coding	0.087	0.1006
10	LOC399947 (399947) 11:108798 kb; protein-coding	4.9584	2.7673
11	CXCL6 (6372) 4:74921 kb; protein-coding	4.811	5.8899
12	ARMCX2 (9823) 23:100797 kb; protein-coding	5.0271	3.2145
13	WNT2B (7482) 1:112812 kb; protein-coding	4.2883	3.126
14	RCN3 (57333) 19:54723 kb; protein-coding	4.6319	2.9803
15	CXCL1 (2919) 4:74954 kb; protein-coding	5.3778	3.8951
16	IL8 (3576) 4:74825 kb; protein-coding	4.4047	3.6682
17	LPPR4 (9890) 1:99502 kb; protein-coding	5.5574	3.3825
18	TNFRSF11B (4982) 8:120005 kb; protein-coding	5.635	4.2706
19	PRSS35 (167681) 6:84279 kb; protein-coding	5.5395	4.0118
20	OAS3 (4940) 12:111861 kb; protein-coding	6.9024	2.8608
21	ANPEP (290) 15:88129 kb; protein-coding	7.3877	3.5788
22	CLEC3B (7123) 3:45043 kb; protein-coding	8.6082	3.0183
23	IFI44L (10964) 1:78859 kb; protein-coding	8.9456	3.938

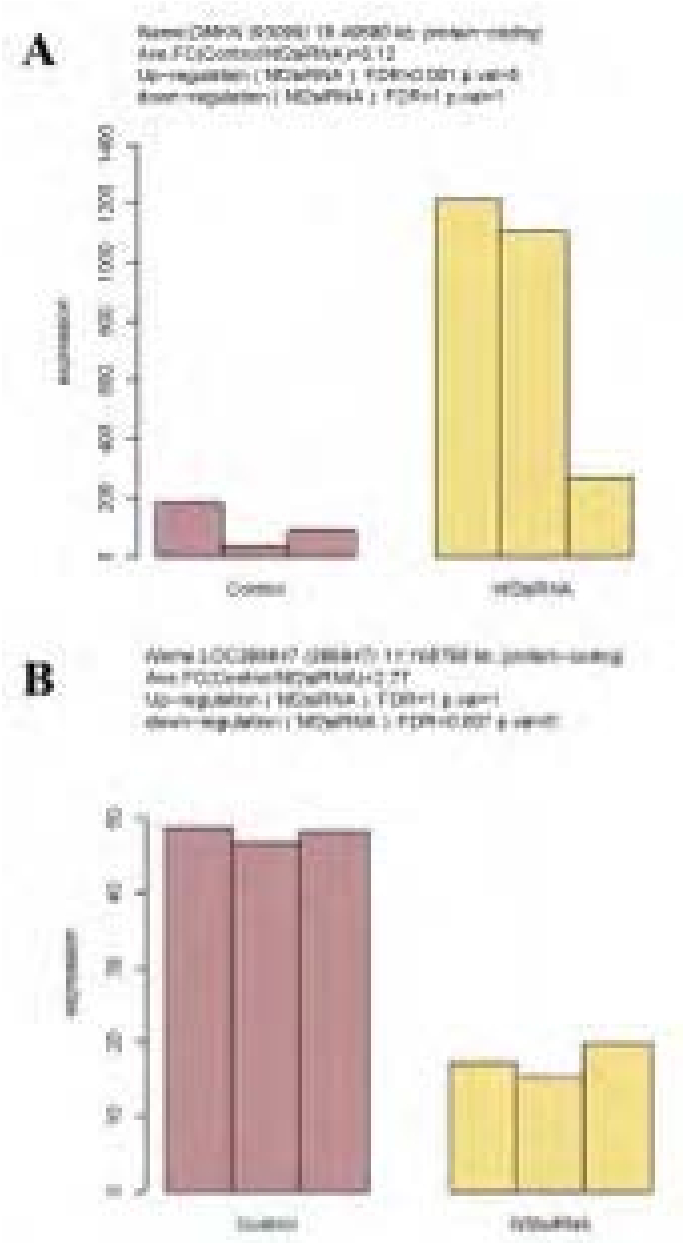

Figure 4. Expression of Two Merlin Target Genes in MENII-1. Expression of DMKN (A) is induced in response to merlin loss while the expression of LOC399947 is reduced in response to merlin loss in MENII-1 cells. The purple bars are triplicate microarray analysis performed on MENII-1-Control cells and the yellow bars are triplicate microarray analysis performed on MENII-1-NF2 siRNA cells. Both these 2 genes and 21 other genes listed in Table 1 were similarly altered in AC1 cells.

NEOPLASIA
www.neoplasia.com

Volume 10 Number 11 November 2008 pp. 1204–1212 1204

The Neurofibromatosis 2 Tumor Suppressor Gene Product, Merlin, Regulates Human Meningioma Cell Growth by Signaling through YAP[1]

Katherine Striedinger*, Scott R. VandenBerg*, Gilson S. Baia*, Michael W. McDermott*, David H. Gutmann† and Anita Lal*

*Brain Tumor Research Center, Department of Neurological Surgery, University of California, San Francisco, CA 94143, USA; †Department of Neurology, Washington University School of Medicine, St. Louis, MO 63110, USA

Abstract

Neurofibromatosis type 2 (NF2) is an autosomal dominant disorder characterized by the occurrence of schwannomas and meningiomas. Several studies have examined the ability of the *NF2* gene product, merlin, to function as a tumor suppressor in diverse cell types; however, little is known about merlin growth regulation in meningiomas. In *Drosophila*, merlin controls cell proliferation and apoptosis by signaling through the Hippo pathway to inhibit the function of the transcriptional coactivator Yorkie. The Hippo pathway is conserved in mammals. On the basis of these observations, we developed human meningioma cell lines matched for merlin expression to evaluate merlin growth regulation and investigate the relationship between *NF2* status and Yes-associated protein (YAP), the mammalian homolog of Yorkie. *NF2* loss in meningioma cells was associated with loss of contact-dependent growth inhibition, enhanced anchorage-independent growth and increased cell proliferation due to increased S-phase entry. In addition, merlin loss in both meningioma cell lines and primary tumors resulted in increased YAP expression and nuclear localization. Finally, siRNA-mediated reduction of YAP in *NF2*-deficient meningioma cells rescued the effects of merlin loss on cell proliferation and S-phase entry. Collectively, these results represent the first demonstration that merlin regulates cell growth in human cancer cells by suppressing YAP.

Neoplasia (2008) 10, 1204–1212

Introduction

Neurofibromatosis type 2 (NF2) is a cancer predisposition syndrome phenotypically characterized by the occurrence of multiple nervous system tumors. The two most common tumors in this inherited syndrome are schwannomas and meningiomas [1]. Whereas meningiomas from individuals with NF2 exhibit biallelic inactivation of the *NF2* gene, loss of *NF2* expression is also detected in as many as 60% of sporadic meningiomas [2]. Similarly, genetically engineered mice with leptomeningeal *NF2* inactivation also develop meningiomas [3,4]. These findings strongly implicate the *NF2* gene in the pathogenesis of meningiomas; however, the molecular mechanism by which *NF2* regulates cell growth relevant to meningioma tumorigenesis remains unsolved.

Merlin (or schwannomin), the product of the *NF2* gene, is a member of the protein 4.1 family that links the actin cytoskeleton to plasma membrane proteins [5]. Although few studies have examined merlin loss in meningioma cells, loss of merlin in fibroblasts and Schwann cells results in loss of contact-dependent inhibition of proliferation, enhanced growth in soft agar and tumor formation in mice [6,7]. In these cell types, merlin has been implicated in epidermal growth factor receptor [8], β_1-integrin [9], and CD44 [7] function as well as Ras [10], Rac1 [11,12], phosphatidylinositol 3-kinase [13], mitogen-activated protein kinase [14], and signal transducer and activator of transcription [15] intracellular signaling. It is not known whether any of these growth control pathways are deregulated in *NF2*-deficient meningioma tumors.

Negative regulation of growth by merlin is conserved in *Drosophila*, where it acts upstream of the Hippo signaling pathway to coordinately

Address all correspondence to: Anita Lal, Brain Tumor Research Center, Department of Neurological Surgery, Box 0520, University of California, San Francisco, CA-94143. E-mail: anita.lal@ucsf.edu

[1]Grant support: Department of Defense New Investigator Award (W81XWH-06-1-0221) and Concept Award (NF073066) to A. Lal and Department of Defense Award to D. Gutmann.
Received 29 May 2008; Revised 4 August 2008; Accepted 5 August 2008

DOI 10.1593/neo.08642

regulate cell proliferation and apoptosis [16,17]. Mutations in merlin or other components of the Hippo pathway such as the serine/threonine kinases, Hippo and Warts, the adaptor molecule, Salvador, or Mats, results in activation of the transcriptional coactivator, Yorkie. Yorkie regulates expression of downstream target genes including *cyclin E* and *DIAP1* (*Drosophila* inhibitor of apoptosis protein 1) causing increased growth, delayed cell cycle exit, inhibition of apoptosis, and enhanced cell survival [16,17].

Individual components of the Hippo pathway are highly conserved in mammals, where they also regulate cell proliferation and apoptosis (Figure 1) [18,19]. Mice and humans have two Warts orthologs, Lats1 and Lats2. Mice deficient for Lats1 develop soft-tissue sarcomas and ovarian tumors [20]. The human ortholog of Salvador, hWW45, is mutated in cancer cell lines [21]. The two mammalian Hippo homologues, Mst1 and Mst2, promote apoptosis and regulate cell cycle exit [22]. Vertebrate Mst2 can rescue the lethality and overgrowth phenotypes of Hippo mutants in *Drosophila* [23]. Similar to their *Drosophila* counterparts, human Mst2 phosphorylates and activates both Lats1 and Lats2 [24]. The Yes-associated protein (YAP), the mammalian ortholog of Yorkie, is the primary effector of the mammalian Hippo pathway. Similar to the function of Yorkie in *Drosophila*, YAP causes aberrant tissue expansion in mice and induces epithelial transformation in mammary cells [25,26].

Given the conservation of components and mechanisms that operate downstream of merlin between *Drosophila* and mammals, we tested the functional relationship among merlin, Hippo pathway regulation, and growth suppression in human meningioma tumors. We developed nonneoplastic and neoplastic meningeal cell lines that mimic gain or loss of *NF2* expression and used these matched lines to examine merlin regulation of YAP. We found that absence of merlin results in loss of contact-dependent inhibition of growth and promotes anchorage-independent growth. Merlin loss enhances cell proliferation by increasing entry into the S-phase and cyclin E1 expression. Inactivation of merlin results in increased YAP expression and nuclear accumulation of YAP in these meningioma cell lines and in primary human meningioma tumors. Finally, we show that YAP suppression reverses the proliferation effects associated with merlin loss in meningiomas. Collectively, these data demonstrate that merlin regulates cell growth in a YAP-dependent manner in meningiomas and suggests that YAP is a compelling target for therapeutic inhibition of human meningioma tumor growth.

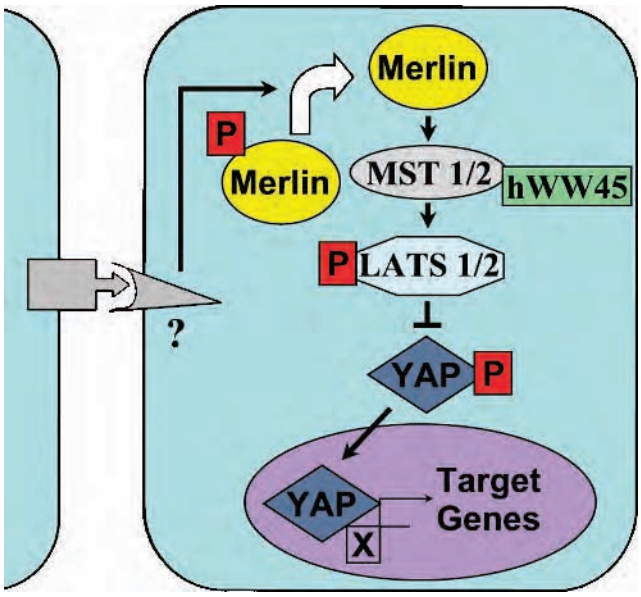

Figure 1. Schematic of the mammalian Hippo signaling pathway. The Hippo pathway is an evolutionary conserved cellular pathway that coordinately regulates cell proliferation and apoptosis. Merlin has been proposed to interact with unknown membrane proteins and transduce a signal that stimulates the phosphorylation of LATS1/2 by the serine/threonine kinases MST1/2 that interact with hWW45. LATS1/2 inhibits the transcriptional coactivator YAP resulting in suppressed expression of downstream target genes such as cyclins that are involved in cell growth and proliferation.

Materials and Methods

Tumor Samples, Cell Lines, and Culture

All human meningioma tumor samples were collected by the Neurological Surgery Tissue Bank using protocols approved by the University of California, San Francisco Committee on Human Research. Human meningioma cell lines used were KT21MG1 [27] and MENII-1. MENII-1 cells were isolated from a surgically resected grade II meningioma and were immortalized by the expression of telomerase and the human papillomavirus *E6/E7* genes as described earlier [28]. Human arachnoidal cells (AC1) were cultured by plating small fragments of surgically resected spinal arachnoid tissue on scores scratched on the bottom of six-well tissue culture plates. Within 7 days, cells with characteristic arachnoidal morphology growing as a monolayer of polygonal cells with large cytoplasmic arcs migrate out of these scores. The arachnoidal origins of these cells were verified by positive staining for vimentin and desmoplakin. Primary cultures of arachnoidal cells were immortalized by stable transfection with the human papillomavirus *E6/E7* oncogenes and telomerase as described earlier [28]. All cell lines were maintained in Dulbecco's modified Eagle's medium supplemented with 10% fetal bovine serum and appropriate antibiotic selection markers.

Expression Constructs and Antibodies

The pSUPER.retro.neo-*NF2*-siRNA construct was generated by digesting the pSUPER.retro.neo vector (Oligoengine) with *Bgl*II and *Hind*III and ligating the annealed oligos (5′-gatccccGCAGCAAGCACAATACCATttcaagagaATGGTATTGTGCTTGCTGCttttta and 5′-agcttaaaaaGCAGCAAGCACAATACCATtctcttgaaATGGTATTGTGCTTGCTGCggg) that contain a 19-nucleotide *NF2* target sequence (in caps) using the strategy described earlier [29]. The pSUPER.retro.neo-YAP-siRNA construct was also generated in pSUPER.retro.neo using the strategy described above and a previously described YAP target sequence (CCAGAGAATCAGTCAGAGA) [30]. A nonspecific mammalian scramble sequence (Oligoengine, Seattle, WA) in pSUPER.retro.neo (pSUPER.retro.neo-Control) was used as a control for the development of stable cell lines. Wild type *NF2*, S518A *NF2*, and S518D *NF2* mutant constructs in pUHD10.3 have been previously described [7,31]. These three constructs were subcloned into pBABE-Hygro using standard techniques. Merlin polyclonal (A19, #sc-331) and monoclonal (B12, #sc-55575) antibodies and the cyclin E1 monoclonal antibody (13A3, #sc-56310) were from Santa Cruz Biotechnology, Santa Cruz, CA. The YAP monoclonal antibody (#4912) was from Cell Signaling (Danvers, MA), the cyclin D1 monoclonal antibody

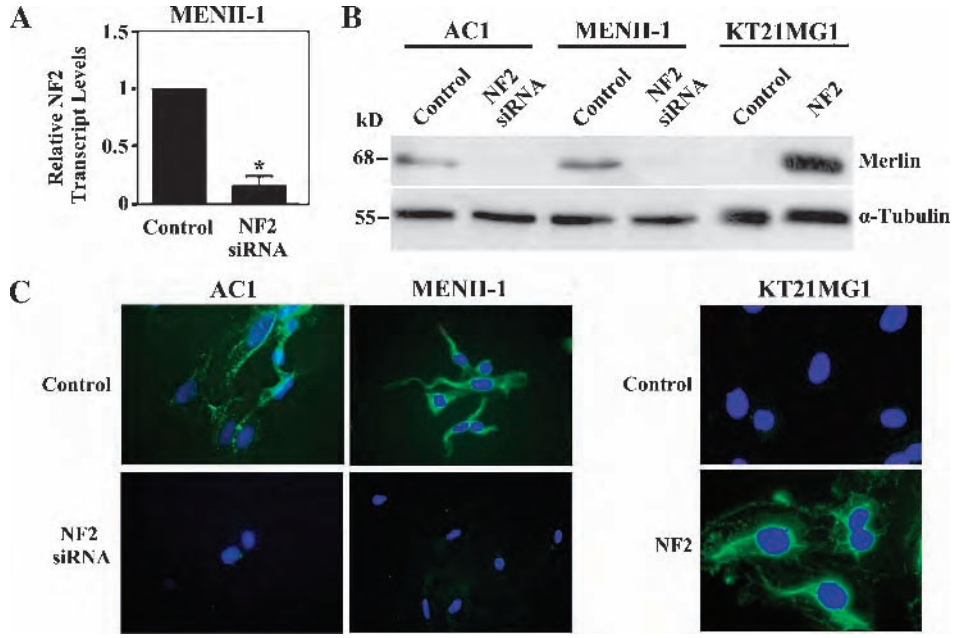

Figure 2. *In vitro* model system of merlin expression in human meningeal cells. Endogenous merlin was silenced in AC1 and MENII-1 cells using *NF2* specific siRNA. In parallel, merlin isoform 1 was exogenously expressed in KT21MG1 cells using retroviral mediated gene transfer. (A) *NF2* transcript levels were measured by quantitative PCR and showed a 5.6-fold reduction in MENII-1-*NF2*-siRNA cells compared with MENII-1-Control cells. Asterisk denotes statistical significance ($P < .05$). (B) Western blot analysis of cell lysates derived from AC1, MENII-1, and KT21MG1 stable cell populations was used to confirm loss or gain of merlin. Whereas merlin expression was observed in AC1-Control and MENII-1-Control cells, *NF2* siRNA abolished expression of merlin in AC1-*NF2*-siRNA and MENII-1-*NF2*-siRNA cells. In parallel, KT21MG1-Control cells lacked merlin, whereas KT21MG1-NF2 cells expressed wild type merlin. Levels of α-tubulin were determined in the same samples as a loading control. Immunoblot of one representative experiment of three with similar results is shown. (C) Immunofluorescence using the A19 polyclonal antibody against merlin revealed the presence of cytoplasmic staining in AC1-Control and MENII-1-Control cells and its absence in AC1-*NF2*-siRNA and MENII-1-*NF2*-siRNA cells. In contrast, KT21MG1-Control cells had no staining, whereas KT21MG1-*NF2* cells had cytoplasmic staining. Merlin immunolabeling is shown in green, and nuclear DAPI counterstaining is shown in blue.

(clone DCS-6) was from BD Pharmingen (Franklin Lakes, NJ), and the α-tubulin (#CP06) antibody was from Calbiochem (San Diego, CA).

Retroviral Infection and Selection of Stable Cell Populations

To stably suppress *NF2* in MENII-1 and AC1 cell lines, retroviral supernatants were generated by transfecting Phoenix A packaging cells with pSUPER.retro.neo-*NF2*-siRNA or pSUPER.retro.neo-Control using Lipofectamine 2000 Plus Reagent (Invitrogen, Carlsbad, CA). The 48-hour posttransfection supernatant was harvested, filtered, and used to infect MENII-1 and AC1 cell lines in the presence of 8 μg/ml polybrene. Stable cell populations were selected using 500 μg/ml G418. In parallel, stable cell populations expressing wild type or mutant *NF2* were generated by transfecting Phoenix A cells with the particular pBABE-Hygro construct and infecting KT21MG1 cells with the 48-hour posttransfection supernatant. Stable cell populations were selected using 200 μg/ml hygromycin. Empty pBABE-Hygro vector was used as a negative control.

Transient Suppression of YAP

Merlin-positive and -negative MENII-1 stable cell populations generated above were plated at 80% confluency in 100-mm dishes and transfected with 10 μg of pSUPER.retro.neo-YAP siRNA using Lipofectamine 2000 Plus Reagent (Invitrogen). Empty pSUPER.retro.neo vector was used as a negative control. The 72-hour posttransfection cells were subjected to flow cytometry to quantify bromodeoxyuridine (BrdU) uptake (described below).

Quantitative Polymerase Chain Reaction

Quantitative polymerase chain reaction (PCR) was performed in three independent experiments using cDNA templates with the I-cycler machine (Bio-Rad, Hercules, CA) and SYBR Green I (Molecular Probes, Eugene, OR) using PCR conditions and data analysis as described earlier [32]. Primers specific for GAPDH and actin were used to verify the integrity of the cDNA and to normalize cDNA yields. The primers used were: GAPDH, 5′-GGAAGCTTGTCATCAATGGAA and 5′-AAATGAGCCCCAGCCTTCTC; Actin, 5′-CAGGAGGAGCAATGATCTTG and 5′-ACTCTTCCAGCCTTCCTTCC; NF2, 5′-ACCGTTGCCTCCTGACATAC and 5′-TCGGAGTTCTCATTGTGCAG; YAP, 5′-GCAGTTGGGAGCTGTTTCTC and 5′-GCCATGTTGTTGTCTGATCG; cyclin E1, 5′-CCATCCTTCTCCACCAAAGA and 5′-TTTGATGCCATCCACAGAAA; cyclin D1, 5′-TGTTTGCAAGCAGGACTTTG and 5′-CCTTCCGGTGTGAAACATCT.

Western Blot Analysis

Total cell lysates were prepared either in buffer A (50 mM Tris-HCl, pH 7.5; 1 mM EDTA pH 8.0, 1% Triton) for merlin detection or in 1× SDS buffer following manufacturer's instructions (Cell

Signaling) for YAP and cyclin protein detection. Protein (50-200 μg) was resolved by electrophoresis for each sample and was transferred to a polyvinylidenefluoride membrane. Membranes were blocked in 5% low-fat dry milk in Tris-buffered saline–Tween 20 and incubated overnight at 4°C with either merlin A19 or B12 antibodies, or the YAP, cyclin E1, or cyclin D1 antibody, or α-tubulin. Incubation with horseradish peroxidase–conjugated goat antirabbit or antimouse immunoglobulin (Jackson Immunoresearch, West Grove, PA) was performed for 1 hour at room temperature. Bound antibody was visualized by chemiluminescence using the SuperSignal West Pico substrate (Pierce Chemical Co., Rockford, IL). The molecular weights were determined with the use of prestained protein ladders (BioRad, Hercules, CA, and Invitrogen). Films were scanned and exported as TIFF files.

Immunofluorescence Microscopy

Indirect immunofluorescence for merlin (A19 antibody or B12 antibody) and YAP was performed as described earlier [28]. Briefly, cells were fixed, permeabilized, blocked, and sequentially incubated with primary and secondary (Alexa 488 goat antirabbit IgG or Alexa 546 goat antimouse IgG) antibodies. Cells were mounted in DAPI mounting media, examined, and photographed with a microscope (Zeiss, Thornwood, NY).

Immunohistochemistry

Immunohistochemical staining was performed on 5-μm formalin-fixed, paraffin-embedded sections from meningioma tissue (8 primary tumors) and from a meningioma tissue microarray (29 primary tumors) for merlin (B12 antibody) and YAP as described earlier [33]. Slides were reviewed in consultation with a neuropathologist (S.R.V.) and included 33 WHO grade I and 4 WHO grade III meningiomas.

Growth Curves and Soft Agar Assay

Merlin-positive and -negative stable cell populations (20,000 cells) were plated in 24-well plates, and cells from three wells were counted at 3, 6, 12, 18, 25, and 30 days. To assess colony growth in soft agar, 50,000 cells were plated in Dulbecco's modified Eagle's medium in 0.4% low melting temperature agarose upon a layer of 0.8% agarose. After 8 weeks, colonies were stained with 0.005% crystal violet, and colonies larger than 100 μm in diameter were scored by counting under a microscope.

Flow Cytometry

Cells (70-80% confluent) were incubated with 1 mM BrdU for 3 hours at 37°C and processed using the fluorescein isothiocyanate BrdU Flow Kit (BD Biosciences, San Jose, CA) following manufacturer's instructions. Briefly, 1×10^6 trypsinized cells were fixed, permeabilized, and digested with DNAse. Cells were then stained with fluorescein isothiocyanate–conjugated anti-BrdU and 7-aminoactinomycin (7-AAD). Flow cytometry was performed on a Becton Dickinson FACSCalibur machine. For each experiment, 10,000 events were counted. Data acquisition was performed with the CellQuest software (BD Biosciences), and data were analyzed using Flow Jo v8.5.3.

Statistics

All data are expressed as mean ± SEM. GraphPad Prism version 4 was used for statistical analysis, consisting of unpaired *t* test and significant differences with a $P < .05$.

Results

Establishment of Matched NF2-Expressing and NF2-Deficient Human Arachnoidal and Meningioma Cell Lines

To develop a meningioma-specific NF2 *in vitro* model system, we determined the expression levels of endogenous merlin in normal human arachnoidal and meningioma cell lines (data not shown). On the basis of these results, we selected one arachnoidal cell line (AC1), one merlin-positive grade II meningioma cell line (MENII-1), and one merlin-negative grade III meningioma cell line (KT21MG1) for further analysis. Paired cell lines were generated by either suppressing *NF2* expression in AC1 and MENII-1 cells using RNA interference (siRNA) or by overexpressing the full-length human *NF2* cDNA (isoform 1, lacking exon 16 sequences) in KT21MG1 cells after retroviral-mediated gene transfer. Stable cell populations expressing either *NF2* siRNA (AC1-*NF2*-siRNA or MENII-1-*NF2*-siRNA) or a nonspecific target siRNA (AC1-Control or MENII-1-Control) were

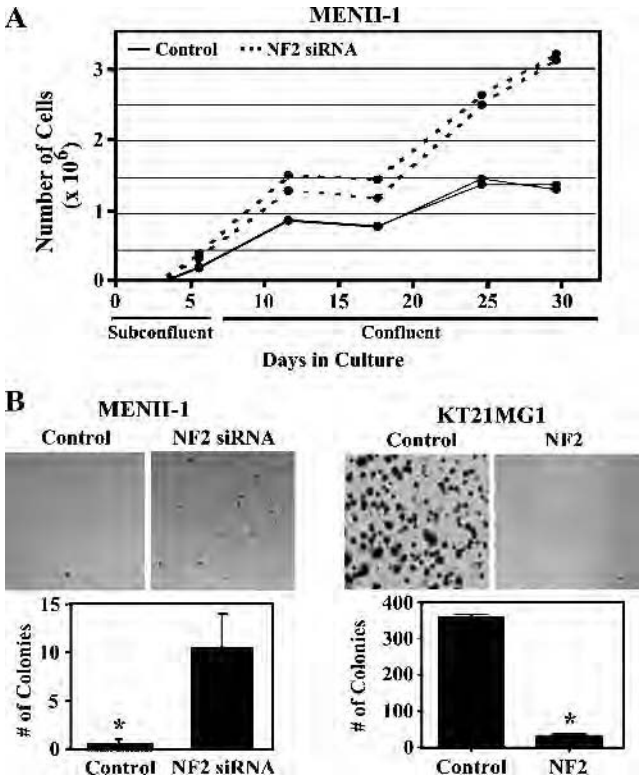

Figure 3. Suppression of merlin causes loss of contact-dependent inhibition of growth and promotes anchorage-independent growth. (A) Growth curves in the presence and absence of merlin expression. Cultures were subconfluent during the first 6 days. MENII-1-*NF2*-siRNA cells (*dotted lines*) continued growing after confluent conditions and have less contact-dependent inhibition of growth compared with MENII-1-Control cells (*solid lines*). Each line corresponds to representative cultures. (B) *NF2* suppression promotes anchorage-independent growth. Marked increased in colony formation in soft agar was observed in cells without merlin expression as MENII-1-*NF2*-siRNA and KT21MG1-Control cells compared with MENII-1-Control and KT21MG1-*NF2*, respectively. Representative images of the colonies formed (*upper panel*) and the mean number of colonies per well (*lower panel*) are shown. Error bars equal ±SE of three independent experiments. Asterisks denote statistical significance ($P < .05$).

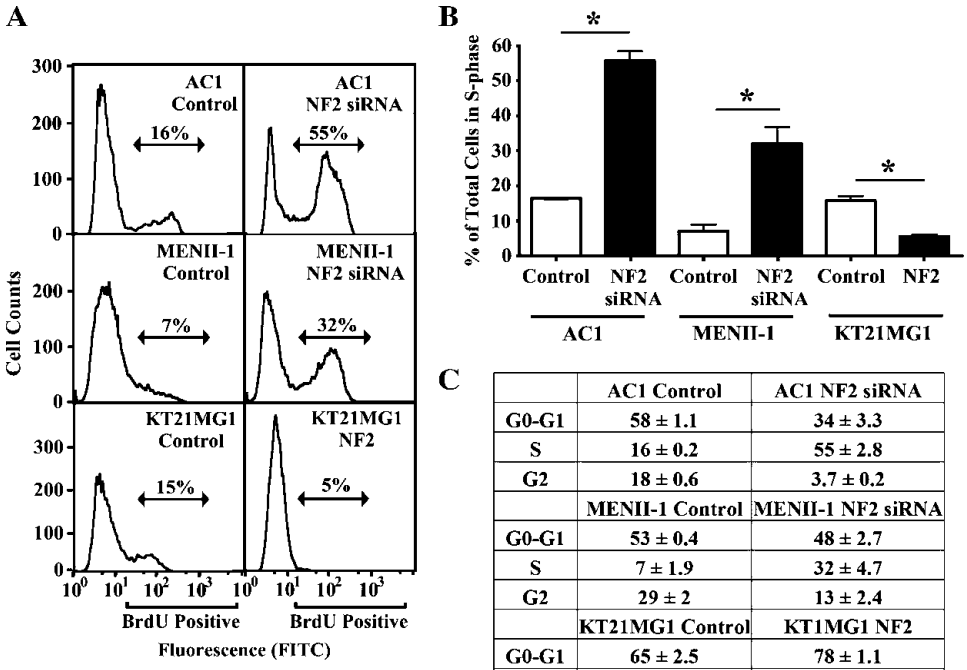

C

	AC1 Control	AC1 NF2 siRNA
G0-G1	58 ± 1.1	34 ± 3.3
S	16 ± 0.2	55 ± 2.8
G2	18 ± 0.6	3.7 ± 0.2
	MENII-1 Control	MENII-1 NF2 siRNA
G0-G1	53 ± 0.4	48 ± 2.7
S	7 ± 1.9	32 ± 4.7
G2	29 ± 2	13 ± 2.4
	KT21MG1 Control	KT1MG1 NF2
G0-G1	65 ± 2.5	78 ± 1.1
S	15 ± 1.2	5 ± 0.6
G2	7.6 ± 0.7	7 ± 0.07

Figure 4. Merlin loss enhances S-phase entry. AC1 and meningioma cell lines (MENII-1 and KT21MG1) were labeled with BrdU and 7-AAD to assess the cell cycle distribution of individual cells by flow cytometry. (A) Representative flow cytometric histograms indicate an increase in the percent of BrdU-positive cells in AC1-*NF2*-siRNA, MENII-1-*NF2*-siRNA, and KT21MG1-Control cells compared with AC1-Control, MENII-1-Control, and KT21MG1-*NF2* cells, respectively. (B) Bar graphs depict the percentage of cells in the S-phase of the cell cycle (BrdU-positive cells) averaged from three independent experiments. Error bars correspond to ±SE. Asterisks denote statistical significance using unpaired *t* test ($P < .05$). (C) Table shows the mean of the percentage of cells ±SE in each phase of the cell cycle from three independent experiments.

selected. *NF2* transcript levels were 5.6-fold lower in MENII-1-*NF2*-siRNA cells when compared with MENII-1-Control cells using quantitative PCR (Figure 2*A*). Similarly, merlin protein expression was undetectable in AC1-*NF2*-siRNA and MENII-1-*NF2*-siRNA cells by Western blot analysis and immunofluorescence (Figure 2, *B* and *C*). In parallel, stable cell populations expressing either exogenous merlin (KT21MG1-*NF2*) or empty vector (KT21MG1-Control) were selected. Expression of merlin in KT21MG1-*NF2* cells was confirmed by Western blot and immunofluorescence (Figure 2, *B* and *C*). In total, we have generated three separate human meningeal and meningioma cell lines that differ only in their expression of merlin for subsequent study.

Merlin Loss Increases S-Phase Entry, Cell Proliferation, and Promotes Anchorage-Independent Growth

Next, we assessed the effect of merlin loss on the growth properties of these human meningioma cell lines. MENII-1-*NF2*-siRNA cells exhibited a more pronounced loss of contact-dependent inhibition of growth compared with MENII-1-Control cells (Figure 3*A*). Merlin loss also promoted colony formation in soft agar. In these experiments, MENII-1-*NF2*-siRNA cells formed a greater number of colonies (10.6 ± 3.2) larger than 100 μm in diameter compared with MENII-1-Control cells (0.4 ± 0.4; $P = .01$; Figure 3*B*). Conversely, merlin expression in KT21MG1 cells significantly decreased the formation of colonies (32 ± 6.3) compared with merlin-negative KT21MG1 cells (361 ± 4.9; $P \leq .0001$; Figure 3*B*).

To determine the effect of merlin on cell cycle progression, we measured BrdU incorporation and total DNA content by flow cytometry. Loss of merlin in AC1 and MENII-1 cells resulted in a significant increase in the percentage of BrdU-positive cells, indicated by an increase in S-phase entry (Figure 4). This is consistent with the observed increase in proliferation in *NF2*-deficient cells. Conversely, expression of exogenous merlin in KT21MG1 cells induced G_0/G_1 arrest and a concomitant decrease in the S-phase cell population (Figure 4). These results demonstrate that merlin functions as a negative growth regulator for both nonneoplastic leptomeningeal cells and meningioma cells and establishes this system as a tractable experimental platform for examining growth regulatory pathways.

Merlin Loss Is Associated with an Increase in YAP Protein Expression

In *Drosophila*, merlin controls cell proliferation and apoptosis by signaling through the Hippo pathway and its effector protein Yorkie, the ortholog of YAP [16,18]. To determine whether merlin might regulate meningioma cell growth by modulating Hippo pathway signaling, we investigated whether changes in merlin expression were associated with altered levels of YAP using our human NF2 meningioma model system. Transcript levels of YAP were unaffected by merlin loss in MENII-1 cells (data not shown); however, YAP protein expression was elevated in arachnoidal and meningioma cells lacking merlin expression and decreased in KT21MG1 cells expressing wild type merlin (Figure 5*A*). These results suggest that merlin regulates YAP expression at the translational or posttranslational level.

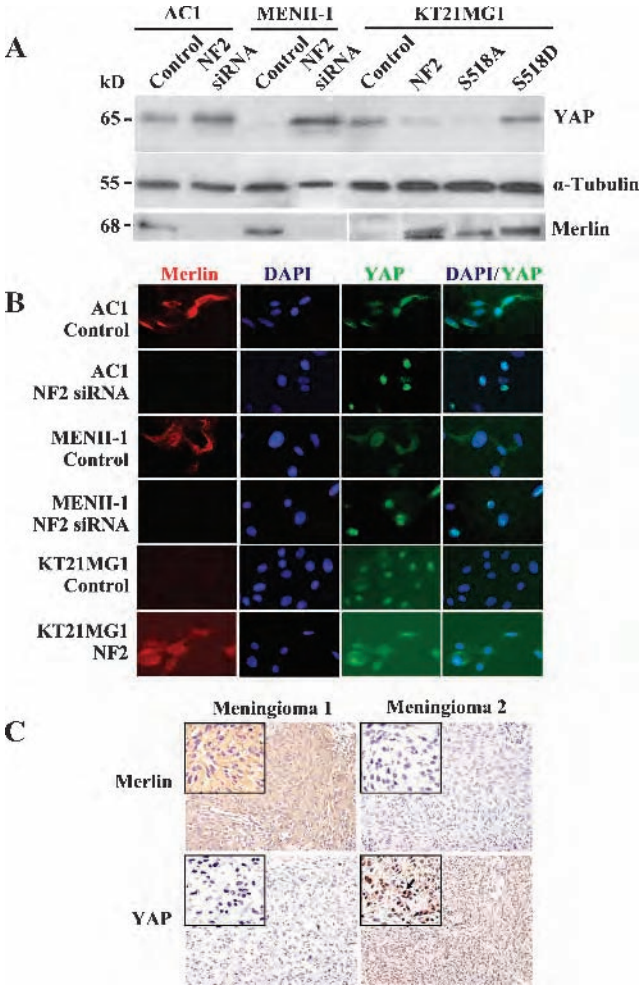

Figure 5. Protein levels of YAP are up-regulated and localized to the nucleus in *NF2*-deficient cells. (A) Total cell lysates were subjected to Western blot using a YAP- or merlin-specific antibody. Increased YAP protein expression was observed when *NF2* was suppressed in AC1 and MENII-1 cells compared with controls. Conversely, exogenous expression of merlin decreased YAP in KT21MG1 cells compared with controls. Expression of a nonphosphorylated, active merlin (S518A *NF2*) was also associated with lower levels of YAP compared with the expression of pseudophosphorylated inactive merlin (S518D *NF2*). Levels of α-tubulin were determined in the same samples as loading control. Results were reproduced in three independent experiments. (B) YAP was translocated to the nucleus in merlin-deficient cells. Immunofluorescence staining was used to show that YAP was localized to the nucleus in AC1-*NF2*-siRNA, MENII-1-*NF2*-siRNA, and KT21MG1-Control cells. In contrast, YAP was primarily cytoplasmic in AC1-Control, MENII-1-Control, and KT21MG1-*NF2* cells. Merlin immunolabeling is shown in red; YAP staining is shown in green; and nuclear DAPI counterstaining is shown in blue. (C) *In situ* immunostaining of merlin and YAP in serial sections of primary human meningioma tumors. We surveyed 37 primary meningiomas by immunohistochemistry. YAP expression was minimal to absent in 95% of merlin-positive meningiomas (a representative tumor is shown here as *Meningioma 1*). In contrast, YAP was expressed and localized to the nucleus in 92% of merlin-negative meningiomas (a representative tumor is shown here as *Meningioma 2*). Arrow depicts an example of YAP nuclear localization. Insets show images at higher magnification.

Merlin becomes active after dephosphorylation of the conserved C-terminal serine 518 (S518) residue [31,34]. Previous studies have shown that merlin mutants in which this phosphorylatable residue is changed to alanine (S518A) are constitutively nonphosphorylated and active, whereas those containing aspartic acid (S518D) are pseudophosphorylated and nonfunctional as negative growth regulators [31,34]. Using these mutants, we assessed the effect of merlin phosphorylation status on YAP protein levels in KT21MG1 human meningioma cells. YAP protein levels were markedly up-regulated in KT21MG1 cells expressing the S518D inactive mutant compared with those with active merlin S518A expression (Figure 5*A*), suggesting that active and functional merlin was required to inhibit YAP.

YAP has been reported to shuttle between the cytoplasm and the nucleus where it can function as a transcriptional coactivator [35]. To determine whether merlin regulates the subcellular localization of YAP, we used fluorescence immunocytochemistry to examine *NF2*-deficient and *NF2*-expressing AC1 and MENII-1 cells. YAP was preferentially expressed in the cytoplasm of AC1-Control and MENII-1-Control cells. In contrast, YAP was localized in the nucleus in AC1-*NF2*-siRNA and MENII-1-*NF2*-siRNA cells (Figure 5*B*). Collectively, these data indicate that merlin regulates YAP protein expression and YAP nuclear localization.

To assess whether a similar association exists between merlin and YAP in human meningioma tumors, we surveyed 37 sporadic primary meningioma tumors by immunohistochemistry. After immunostaining with a merlin-specific monoclonal antibody, meningiomas were classified as either merlin-positive, if tumors exhibited any positive immunoreactivity, or merlin-negative, if tumors had no immunoreactivity. We then assessed protein levels of YAP in adjacent serial sections. 13 (92%) of 14 merlin-negative meningiomas exhibited strong nuclear YAP immunoreactivity. In contrast, 22 (95%) of 23 merlin-positive meningiomas had weak to no YAP immunoreactivity (Figure 5*C*). These results further support the *in vitro* results demonstrating that merlin regulates YAP protein levels *in vivo*.

Merlin Loss Is Associated with an Increase in Protein Levels of Cyclin E1

Previous studies have identified cyclin E1 as a transcriptional target of the Hippo pathway in *Drosophila* [36–38] and an essential regulator of progression from G_1 to S cell cycle progression in mammalian cells [39,40]. Also, merlin has been reported to inhibit cell proliferation by repressing cyclin D1 in human mesothelioma cells [41]. To determine whether merlin regulates cyclin E1 and/or cyclin D1 levels in human meningioma cells, we measured cyclin E1 and D1 RNA and protein expression by quantitative PCR and Western blot analysis, respectively. Cyclin E1 transcript levels were at least 2.5-fold higher in MENII-1-*NF2*-siRNA cells compared with MENII-1-Control cells, whereas cyclin D1 transcript levels were the same in MENII-1-*NF2*-siRNA and MENII-1-Control cells (Figure 6*A*). In addition, cyclin E1 protein levels were elevated in MENII-1-*NF2*-siRNA and AC1-*NF2*-siRNA cells compared with MENII-1-Control and AC1-Control cells, respectively (Figure 6*B*). Conversely, exogenous expression of merlin in NF2-deficient KT21MG1 cells resulted in decreased cyclin E1 protein levels. In contrast, cyclin D1 protein levels were unaffected by the absence or presence of merlin in both MENII-1 and KT21MG1 cells (Figure 6*C*). These data suggest that merlin likely regulates cell

growth by modulating cyclin E1 expression at the transcriptional level in meningiomas.

YAP Reduction Reverses the Growth Phenotype Associated with Merlin Loss

Lastly, to determine whether YAP expression is necessary for the enhanced S-phase entry induced by merlin loss in meningioma cells, we transiently depleted YAP using RNA interference in MENII-1-Control and MENII-1-*NF2*-siRNA cells (Figure 7). Reduced YAP expression in *NF2*-deficient MENII-1 meningioma cells caused a ~50% decrease in the percentage of cells in S-phase (9 ± 1.2) compared with mock-transfected cells (20 ± 0.2; $P = .001$; Figure 7, *B* and *C*). In contrast, YAP siRNA treatment had a minor effect on MENII-1-Control cells (~20% reduction; $P = .08$; Figure 7, *B* and *C*). Collectively, these experiments demonstrate that YAP transduces the merlin growth regulatory signal in meningiomas and that the Hippo growth control pathway is responsible for merlin tumor suppressor function in this tumor type.

Discussion

The Hippo signaling pathway is emerging as an evolutionarily conserved mechanism that controls organ size and growth relevant to tumorigenesis [18,37]. In this study, we investigated the functional association between *NF2* gene expression and the downstream effector of the Hippo pathway in human meningiomas. We provide several lines of converging and complementary evidence that merlin functions through YAP in meningiomas. First, using paired meningioma cell lines differing only in *NF2* expression, we show that YAP expression is increased in a dose-response manner upon merlin loss. This regulation occurs at the translational or posttranslational level and results in YAP nuclear localization. Second, the relationship between merlin expression and YAP nuclear localization is also observed in human surgical meningioma specimens *in vivo*. These observations are consistent with findings made in other solid cancers in which Hippo signaling is deregulated [42]. Third, suppressed YAP expression in merlin-deficient meningioma cells attenuates the cell growth and S-phase cell cycle progression associated with merlin loss. To the best of our knowledge, these results represent the first demonstration that merlin regulates cell growth in human meningioma cells by suppressing YAP, the main Hippo pathway effector protein.

YAP has previously been implicated in other human cancers, including pancreatic ductal adenocarcinoma, and has been shown to function as an oncogene that induces epithelial transformation of mouse mammary cells [26,43]. Nuclear localization of YAP is dependent on the phosphorylation status of a conserved Ser residue and is necessary for its cotranscriptional activator function [35,44]. YAP associates with multiple transcription factors in the nucleus such as p73 and TEAD/TEF [44,45]. ErbB4 receptors have been reported to recruit YAP and relocate to the nucleus to regulate transcription [46,47]. In contrast, LATS1 inactivates YAP oncogenic function by sequestering YAP in the cytoplasm and, consequently, suppressing its transcriptional regulation of cellular genes [35]. Our findings are in accordance with these and suggest that the tumorigenic behavior of meningioma cells is driven in part by YAP nuclear localization and the transcription of genes involved in increased proliferation.

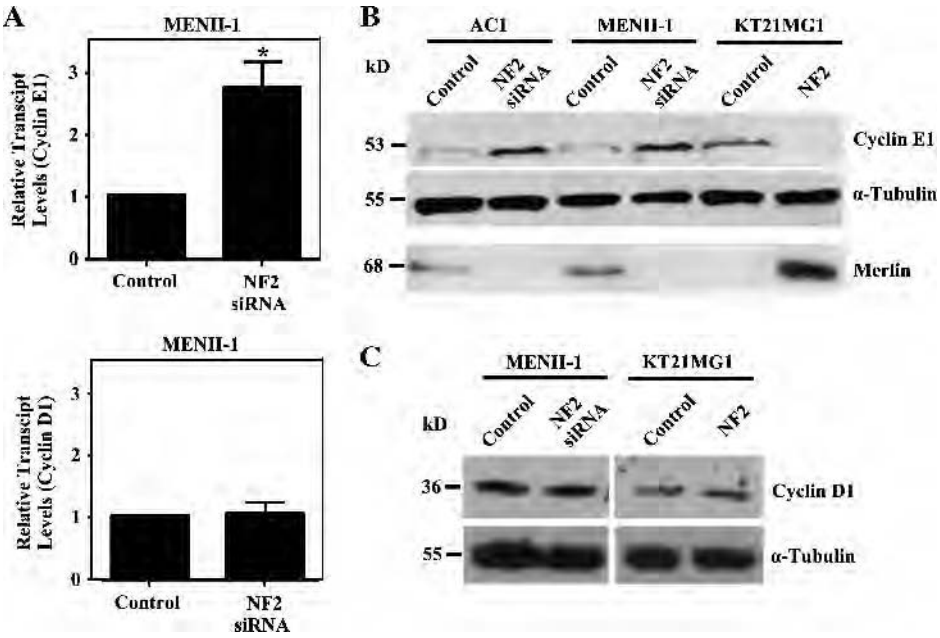

Figure 6. Cyclin E1 and cyclin D1 expression was increased in merlin-deficient cells. (A) Transcript levels of cyclin E1 and cyclin D1 were measured in MENII-1 cells using quantitative PCR. At least a 2.5-fold increase in the transcript levels of cyclin E1 was seen in MENII-1-*NF2*-siRNA cells compared with MENII-1-Control cells, whereas transcript levels of cyclin D1 were unchanged. Asterisk denotes statistical significance ($P < .05$). (B) Western blot analysis of cell lysates derived from AC1, MENII-1, and KT21MG1 stable cells was used to show that protein levels of cyclin E1 were increased in the absence of merlin. Levels of α-tubulin were determined in the same samples as a loading control. (C) Western blot analysis of cell lysates derived from MENII-1 and KT21MG1 stable cells was used to show that protein levels of cyclin D1 were unchanged in the absence of merlin. Levels of α-tubulin were determined in the same samples as a loading control.

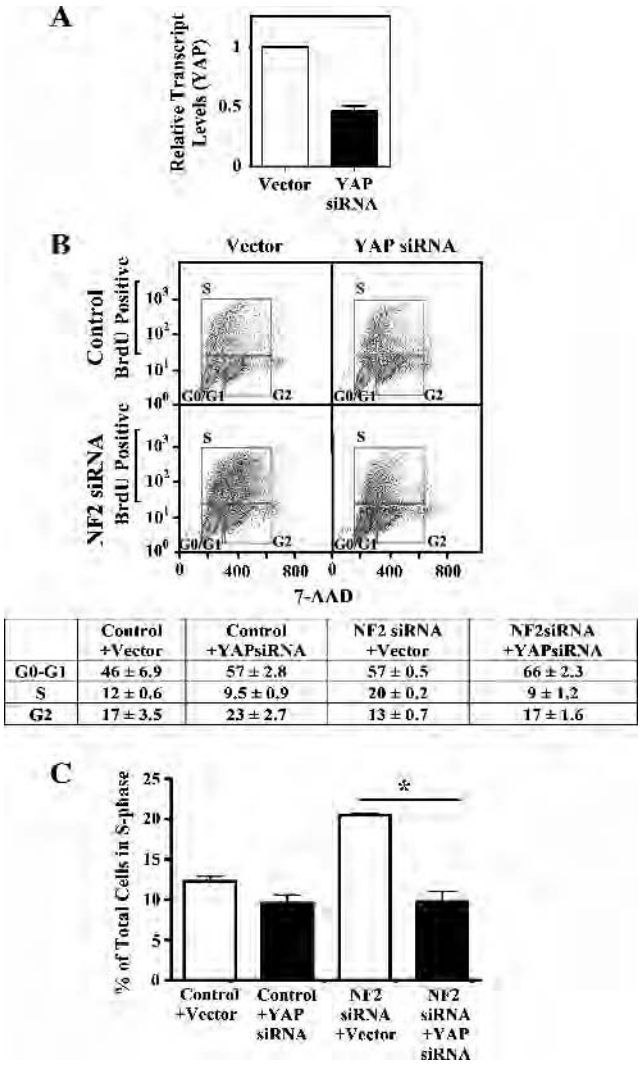

	Control +Vector	Control +YAPsiRNA	NF2 siRNA +Vector	NF2siRNA +YAPsiRNA
G0-G1	46 ± 6.9	57 ± 2.8	57 ± 0.5	66 ± 2.3
S	12 ± 0.6	9.5 ± 0.9	20 ± 0.2	9 ± 1.2
G2	17 ± 3.5	23 ± 2.7	13 ± 0.7	17 ± 1.6

Figure 7. Down-regulation of YAP decreased proliferation in merlin-deficient cells. MENII-1-Control and MENII-1-*NF2*-siRNA cells were transiently transfected with YAP-specific siRNA or empty vector. (A) YAP transcript levels were measured in MENII-1-Control cells using quantitative PCR. The YAP-specific siRNA caused a 50% reduction in YAP transcript levels compared with controls in MENII-1 cells. (B, C) BrdU incorporation and 7-AAD staining were measured by flow cytometry. (B) One representative experiment shows the distribution of cells in G_0-G_1, S, and G_2 phases of the cell cycle. The table below shows the mean of the percentage of cells ±SE in each phase of the cell cycle from three independent experiments. (C) Bar graphs depict the percentage of cells in the S-phase of the cell cycle (BrdU-positive cells) averaged from three independent experiments. Error bars correspond to ±SE. Suppression of YAP decreased the percentage of cells in S-phase in MENII-1-*NF2*-siRNA cells to levels similar to MENII-1-Control cells.

We demonstrate that merlin controls the cell cycle in meningiomas. Merlin suppression results in increased S-phase entry, and merlin expression resulted in G_0/G_1 arrest. Similar results were obtained in mesotheliomas [41] and schwannomas [48]. These results provide strong evidence that merlin functions as a tumor suppressor by controlling the G_0/G_1– to S-phase checkpoint of the cell cycle. Cyclin E1 is thought to be essential for this cell cycle transition in humans [39,40] and has been identified as a downstream target of Yorkie in *Drosophila* [36–38]. In contrast, cyclin E1 was not induced after overexpression of YAP in mammary epithelial cells [26]. Instead, it has been shown that cyclin D1 is regulated by YAP in mouse intestine [25] and by merlin in human mesotheliomas [41]. Our experiments show that merlin regulates cyclin E1 but not cyclin D1 in human meningiomas. These differences most likely represent cell type–specific differences in gene expression. Further studies are needed to determine whether merlin regulates cyclin E1 by signaling through YAP.

The fact that NF2 patients develop only certain CNS tumors also emphasizes the cell type–specific tumorigenic effects of merlin. Merlin loss results specifically in aberrant growth of Schwann and meningeal cell types. However, not all meningiomas have *NF2* loss, suggesting that other mechanisms that do not involve the Hippo pathway result in meningioma formation. Alternatively, it remains to be elucidated whether other components of the Hippo pathway, downstream of merlin, are possibly deregulated in these tumors resulting in the same phenotype as merlin loss.

Treatment strategies for NF2 and sporadic meningioma patients are restricted to traditional forms of cancer therapy such as surgery and radiation therapy. These options are sometimes insufficient because of the location of these tumors, the recurrence despite therapies and the occurrence of multiple tumors. Although receptor tyrosine kinases inhibitors are emerging as pathway targets in other CNS tumors such as glioblastomas [49], targeted therapies have not yet been proposed for meningioma patients. This is mainly because of a lack of knowledge regarding relevant signaling pathways. Our results argue that YAP is an attractive candidate as a key mediator of *NF2* growth regulation and tumorigenesis in meningioma, making it a potential target for the development of therapies for NF2 and meningioma patients.

Acknowledgments

The authors thank the Neurological Surgery Tissue Bank at the University of California, San Francisco, CA, for the primary meningioma tumor samples. The authors also thank Jason Pomerantz for fruitful discussions and critical review of the manuscript.

References

[1] Ferner RE (2007). Neurofibromatosis 1 and neurofibromatosis 2: a twenty first century perspective. *Lancet Neurol* **6**, 340–351.

[2] Ruttledge MH, Sarrazin J, Rangaratnam S, Phelan CM, Twist E, Merel P, Delattre O, Thomas G, Nordenskjold M, Collins VP, et al. (1994). Evidence for the complete inactivation of the *NF2* gene in the majority of sporadic meningiomas. *Nat Genet* **6**, 180–184.

[3] Kalamarides M, Niwa-Kawakita M, Leblois H, Abramowski V, Perricaudet M, Janin A, Thomas G, Gutmann DH, and Giovannini M (2002). *Nf2* gene inactivation in arachnoidal cells is rate-limiting for meningioma development in the mouse. *Genes Dev* **16**, 1060–1065.

[4] Kalamarides M, Stemmer-Rachamimov AO, Takahashi M, Han ZY, Chareyre F, Niwa-Kawakita M, Black PM, Carroll RS, and Giovannini M (2008). Natural history of meningioma development in mice reveals: a synergy of *Nf2* and *p16 (Ink4a)* mutations. *Brain Pathol* **18**, 62–70.

[5] Gautreau A, Louvard D, and Arpin M (2002). ERM proteins and NF2 tumor suppressor: the yin and yang of cortical actin organization and cell growth signaling. *Curr Opin Cell Biol* **14**, 104–109.

[6] Johnson KC, Kissil JL, Fry JL, and Jacks T (2002). Cellular transformation by a FERM domain mutant of the *Nf2* tumor suppressor gene. *Oncogene* **21**, 5990–5997.

[7] Morrison H, Sherman LS, Legg J, Banine F, Isacke C, Haipek CA, Gutmann DH, Ponta H, and Herrlich P (2001). The *NF2* tumor suppressor gene product, merlin, mediates contact inhibition of growth through interactions with CD44. *Genes Dev* **15**, 968–980.

[8] Curto M, Cole BK, Lallemand D, Liu CH, and McClatchey AI (2007). Contact-dependent inhibition of EGFR signaling by Nf2/Merlin. *J Cell Biol* **177**, 893–903.

[9] Fernandez-Valle C, Tang Y, Ricard J, Rodenas-Ruano A, Taylor A, Hackler E, Biggerstaff J, and Iacovelli J (2002). Paxillin binds schwannomin and regulates its density-dependent localization and effect on cell morphology. *Nat Genet* **31**, 354–362.

[10] Tikoo A, Varga M, Ramesh V, Gusella J, and Maruta H (1994). An anti-Ras function of neurofibromatosis type 2 gene product (NF2/Merlin). *J Biol Chem* **269**, 23387–23390.

[11] Shaw RJ, Paez JG, Curto M, Yaktine A, Pruitt WM, Saotome I, O'Bryan JP, Gupta V, Ratner N, Der CJ, et al. (2001). The Nf2 tumor suppressor, merlin, functions in Rac-dependent signaling. *Dev Cell* **1**, 63–72.

[12] Morrison H, Sperka T, Manent J, Giovannini M, Ponta H, and Herrlich P (2007). Merlin/neurofibromatosis type 2 suppresses growth by inhibiting the activation of Ras and Rac. *Cancer Res* **67**, 520–527.

[13] Rong R, Tang X, Gutmann DH, and Ye K (2004). Neurofibromatosis 2 (NF2) tumor suppressor merlin inhibits phosphatidylinositol 3-kinase through binding to PIKE-L. *Proc Natl Acad Sci USA* **101**, 18200–18205.

[14] Chadee DN, Xu D, Hung G, Andalibi A, Lim DJ, Luo Z, Gutmann DH, and Kyriakis JM (2006). Mixed-lineage kinase 3 regulates B-Raf through maintenance of the B-Raf/Raf-1 complex and inhibition by the NF2 tumor suppressor protein. *Proc Natl Acad Sci USA* **103**, 4463–4468.

[15] Scoles DR, Nguyen VD, Qin Y, Sun CX, Morrison H, Gutmann DH, and Pulst SM (2002). Neurofibromatosis 2 (NF2) tumor suppressor schwannomin and its interacting protein HRS regulate STAT signaling. *Hum Mol Genet* **11**, 3179–3189.

[16] Hamaratoglu F, Willecke M, Kango-Singh M, Nolo R, Hyun E, Tao C, Jafar-Nejad H, and Halder G (2006). The tumour-suppressor genes *NF2/Merlin* and *Expanded* act through Hippo signalling to regulate cell proliferation and apoptosis. *Nat Cell Biol* **8**, 27–36.

[17] Harvey K and Tapon N (2007). The Salvador-Warts-Hippo pathway—an emerging tumour-suppressor network. *Nat Rev Cancer* **7**, 182–191.

[18] Dong J, Feldmann G, Huang J, Wu S, Zhang N, Comerford SA, Gayyed MF, Anders RA, Maitra A, and Pan D (2007). Elucidation of a universal size-control mechanism in *Drosophila* and mammals. *Cell* **130**, 1120–1133.

[19] Zeng Q and Hong W (2008). The emerging role of the hippo pathway in cell contact inhibition, organ size control, and cancer development in mammals. *Cancer Cell* **13**, 188–192.

[20] Turenchalk GS, St John MA, Tao W, and Xu T (1999). The role of lats in cell cycle regulation and tumorigenesis. *Biochim Biophys Acta* **1424**, M9–M16.

[21] Tapon N, Harvey KF, Bell DW, Wahrer DC, Schiripo TA, Haber DA, and Hariharan IK (2002). Salvador promotes both cell cycle exit and apoptosis in *Drosophila* and is mutated in human cancer cell lines. *Cell* **110**, 467–478.

[22] Dan I, Watanabe NM, and Kusumi A (2001). The Ste20 group kinases as regulators of MAP kinase cascades. *Trends Cell Biol* **11**, 220–230.

[23] Wu S, Huang J, Dong J, and Pan D (2003). Hippo encodes a Ste-20 family protein kinase that restricts cell proliferation and promotes apoptosis in conjunction with salvador and warts. *Cell* **114**, 445–456.

[24] Chan EH, Nousiainen M, Chalamalasetty RB, Schafer A, Nigg EA, and Sillje HH (2005). The Ste20-like kinase Mst2 activates the human large tumor suppressor kinase Lats1. *Oncogene* **24**, 2076–2086.

[25] Camargo FD, Gokhale S, Johnnidis JB, Fu D, Bell GW, Jaenisch R, and Brummelkamp TR (2007). YAP1 increases organ size and expands undifferentiated progenitor cells. *Curr Biol* **17**, 2054–2060.

[26] Overholtzer M, Zhang J, Smolen GA, Muir B, Li W, Sgroi DC, Deng CX, Brugge JS, and Haber DA (2006). Transforming properties of *YAP*, a candidate oncogene on the chromosome 11q22 amplicon. *Proc Natl Acad Sci USA* **103**, 12405–12410.

[27] Tanaka K, Sato C, Maeda Y, Koike M, Matsutani M, Yamada K, and Miyaki M (1989). Establishment of a human malignant meningioma cell line with amplified *c-myc* oncogene. *Cancer* **64**, 2243–2249.

[28] Baia GS, Slocum AL, Hyer JD, Misra A, Sehati N, Vandenberg SR, Feuerstein BG, Deen DF, McDermott MW, and Lal A (2006). A genetic strategy to overcome the senescence of primary meningioma cell cultures. *J Neurooncol* **78**, 113–121.

[29] Brummelkamp TR, Bernards R, and Agami R (2002). Stable suppression of tumorigenicity by virus-mediated RNA interference. *Cancer Cell* **2**, 243–247.

[30] Levy D, Adamovich Y, Reuven N, and Shaul Y (2007). The Yes-associated protein 1 stabilizes p73 by preventing Itch-mediated ubiquitination of p73. *Cell Death Differ* **14**, 743–751.

[31] Surace EI, Haipek CA, and Gutmann DH (2004). Effect of merlin phosphorylation on neurofibromatosis 2 (NF2) gene function. *Oncogene* **23**, 580–587.

[32] Cuevas IC, Slocum AL, Jun P, Costello JF, Bollen AW, Riggins GJ, McDermott MW, and Lal A (2005). Meningioma transcript profiles reveal deregulated notch signaling pathway. *Cancer Res* **65**, 5070–5075.

[33] Yoo H, Baia GS, Smith JS, McDermott MW, Bollen AW, Vandenberg SR, Lamborn KR, and Lal A (2007). Expression of the hypoxia marker carbonic anhydrase 9 is associated with anaplastic phenotypes in meningiomas. *Clin Cancer Res* **13**, 68–75.

[34] Rong R, Surace EI, Haipek CA, Gutmann DH, and Ye K (2004). Serine 518 phosphorylation modulates merlin intramolecular association and binding to critical effectors important for NF2 growth suppression. *Oncogene* **23**, 8447–8454.

[35] Hao Y, Chun A, Cheung K, Rashidi B, and Yang X (2008). Tumor suppressor LATS1 is a negative regulator of oncogene YAP. *J Biol Chem* **283**, 5496–5509.

[36] Pan D (2007). Hippo signaling in organ size control. *Genes Dev* **21**, 886–897.

[37] Edgar BA (2006). From cell structure to transcription: Hippo forges a new path. *Cell* **124**, 267–273.

[38] Saucedo LJ and Edgar BA (2007). Filling out the Hippo pathway. *Nat Rev Mol Cell Biol* **8**, 613–621.

[39] Ohtsubo M, Theodoras AM, Schumacher J, Roberts JM, and Pagano M (1995). Human cyclin E, a nuclear protein essential for the G_1-to-S phase transition. *Mol Cell Biol* **15**, 2612–2624.

[40] Ohtsubo M and Roberts JM (1993). Cyclin-dependent regulation of G_1 in mammalian fibroblasts. *Science* **259**, 1908–1912.

[41] Xiao GH, Gallagher R, Shetler J, Skele K, Altomare DA, Pestell RG, Jhanwar S, and Testa JR (2005). The *NF2* tumor suppressor gene product, merlin, inhibits cell proliferation and cell cycle progression by repressing cyclin D1 expression. *Mol Cell Biol* **25**, 2384–2394.

[42] Zhao B, Wei X, Li W, Udan RS, Yang Q, Kim J, Xie J, Ikenoue T, Yu J, Li L, et al. (2007). Inactivation of YAP oncoprotein by the Hippo pathway is involved in cell contact inhibition and tissue growth control. *Genes Dev* **21**, 2747–2761.

[43] Guo J, Kleeff J, Zhao Y, Li J, Giese T, Esposito I, Buchler MW, Korc M, and Friess H (2006). Yes-associated protein (YAP65) in relation to Smad7 expression in human pancreatic ductal adenocarcinoma. *Int J Mol Med* **17**, 761–767.

[44] Basu S, Totty NF, Irwin MS, Sudol M, and Downward J (2003). Akt phosphorylates the Yes-associated protein, YAP, to induce interaction with 14-3-3 and attenuation of p73-mediated apoptosis. *Mol Cell* **11**, 11–23.

[45] Vassilev A, Kaneko KJ, Shu H, Zhao Y, and DePamphilis ML (2001). TEAD/TEF transcription factors utilize the activation domain of YAP65, a Src/Yes–associated protein localized in the cytoplasm. *Genes Dev* **15**, 1229–1241.

[46] Omerovic J, Puggioni EM, Napoletano S, Visco V, Fraioli R, Frati L, Gulino A, and Alimandi M (2004). Ligand-regulated association of ErbB-4 to the transcriptional co-activator YAP65 controls transcription at the nuclear level. *Exp Cell Res* **294**, 469–479.

[47] Komuro A, Nagai M, Navin NE, and Sudol M (2003). WW domain-containing protein YAP associates with ErbB-4 and acts as a co-transcriptional activator for the carboxyl-terminal fragment of ErbB-4 that translocates to the nucleus. *J Biol Chem* **278**, 33334–33341.

[48] Schulze KM, Hanemann CO, Muller HW, and Hanenberg H (2002). Transduction of wild-type merlin into human schwannoma cells decreases schwannoma cell growth and induces apoptosis. *Hum Mol Genet* **11**, 69–76.

[49] Stommel JM, Kimmelman AC, Ying H, Nabioullin R, Ponugoti AH, Wiedemeyer R, Stegh AH, Bradner JE, Ligon KL, Brennan C, et al. (2007). Coactivation of receptor tyrosine kinases affects the response of tumor cells to targeted therapies. *Science* **318**, 287–290.

Journal of Neuro-Oncology (2006) 78: 113–121
DOI 10.1007/s11060-005-9076-y

Laboratory Investigation

A genetic strategy to overcome the senescence of primary meningioma cell cultures

Gilson S. Baia[1], Alison L. Slocum[1], Jeanette D. Hyer[1], Anjan Misra[1], Nouzhan Sehati[1], Scott R. VandenBerg[1,2], Burt G. Feuerstein[1,3], Dennis F. Deen[1], Michael W. McDermott[1] and Anita Lal[1]
[1]*Brain Tumor Research Center, Department of Neurological Surgery, University of California, San Francisco, CA, 94143, USA;* [2]*Department of Pathology, University of California, San Francisco, CA, 94143, USA;* [3]*Department of Laboratory Medicine, University of California, 94143, San Francisco, CA, USA*

Key words: immortalization, meningioma, model systems, senescence, telomerase

Summary

Even though meningiomas are the second most common brain tumor in adults, little is known about the molecular basis of their growth and development. The lack of suitable cell culture model systems is an impediment to this understanding. Most studies on meningiomas rely on primary, early passage cell lines that eventually senesce or a few established cell lines that have been derived from aggressive variants of meningiomas. We have isolated three primary meningioma cell lines that are negative for telomerase activity. We can overcome the senescence of a Grade III derived meningioma cell line by expressing the telomerase catalytic subunit (hTERT), whereas Grade I meningioma cell lines require the expression of the human papillomavirus E6 and E7 oncogenes in conjunction with hTERT. Meningioma cell lines, immortalized in this manner, maintain their pre-transfection morphology and form colonies *in vitro*. We have confirmed the meningothelial origin of these cell lines by assessing expression of vimentin and desmoplakin, characteristic markers for meningiomas. Additionally, we have karyotyped these cell lines using array CGH and shown that they represent a spectrum of the genetic diversity seen in primary meningiomas. Thus, these cell lines represent novel cellular reagents for investigating the molecular oncogenesis of meningiomas.

Introduction

Tumor model systems are essential to understand the function of genetic alterations in cancer, to assess their contribution to cancer progression and to serve as preclinical models for evaluating the toxicity and efficacy of conventional and novel therapeutic agents. Cell culture systems are convenient, reproducible and reliable, and they provide an important tool for initial investigations into the cancer of their origin. Meningiomas are the second most common adult brain tumor and are a considerable cause of morbidity and mortality, yet experimental investigations into their biology have been hampered by the lack of appropriate model systems [1]. Most studies on meningiomas have relied on primary, early passage cell lines that usually undergo cellular senescence after a few passages [2–5]. Thus, studies performed using these primary cell lines are not reproducible and characterizations of the cell lines are usually minimal. A few established meningioma cell lines are available and are commonly used by investigators in probing the biology of meningiomas [6, 7]. These cell lines have been derived from aggressive variants of meningiomas. For example, the commonly used meningioma line, IOMM-Lee, was derived from an intraosseous malignant meningioma [6]. While these cell lines are an invaluable resource, there is a need to develop additional cell lines that span the entire spectrum of meningiomas.

The purpose of this study was to overcome the senescence of primary meningioma cell lines and to develop meningioma cell culture model systems that are more characteristic of the majority of clinical meningiomas. Multiple pathways trigger cellular senescence and disruption of these pathways are required for immortalization [8]. Progressive telomere shortening is a primary cause of a finite proliferative life span and a telomere maintenance mechanism has been found in every immortalized cell line examined to date [9]. In the majority of immortalized cell lines and in ~85% of cancers, the enzyme telomerase is activated. In other cancers, telomere length is maintained by an alternative mechanism for lengthening of telomeres (ALT) [10]. Cell cycle checkpoint pathways also control cellular senescence, and cellular immortalization is commonly associated with disruption of the p53 and/or pRb pathways [11]. In fact, intact p53 and pRb pathways can trigger senescence in cells that have a telomere maintenance mechanism [12].

Here, we report that immortalization of a malignant meningioma cell line required expression of hTERT, while immortalization of two benign meningioma cell lines required disruption of the p53 and pRb pathways in addition to expression of hTERT. These immortalized cell lines maintain morphological, immunocytochemical and genetic features characteristic of meningiomas and represent a useful tool for gaining insights into the biology of this type of cancer.

Materials and methods

Cell line generation

Cell lines were established from fresh, viable tumor specimens that were confirmed by routine histopathologic evaluation to be meningiomas, using the 2000 WHO classification and grading system. Viable tissue was placed into Dulbecco's Modified Eagle's Medium supplemented with 10% fetal bovine serum (DME–10%FBS) within 90 s following surgical resection, transported to the lab and dissected into 1 mm pieces. Following digestion with DNAse, Pronase and Collagenase for 30 min at 37 °C, the tissue fragment solution was filtered through a 100-micron filter, and the filtrate centrifuged at 1000 rpm for 10 min to collect dissociated cells. These cells were seeded at a density of 3 to 5×10^6 cells per 100 mm dish and maintained in DME–10%FBS. After achieving 80–90% confluence, the cultures were passaged 1:4. Each passage was considered as two population doublings.

Retroviral infections

Telomerase and E6/E7 expressing stable cell lines were generated using retroviral–mediated gene transfer. pWZL-blast-hTERT or pLXSP-puro-E6/E7 was transfected into the Phoenix A packaging cell line using lipofectamine. The 48 h culture supernatant was used to infect meningioma cell lines in the presence of polybrene (8 μg/ml). Stable cell populations were selected using blasticidin (2 μg/ml) for telomerase expression or puromycin (0.5 μg/ml) for E6/E7 expression.

Telomerase activity

Telomerase activity was detected using the Telomeric Repeat Amplification Protocol (TRAP) assay. TRAP assays were performed using the TRAPeze kit (Intergen, Gaitherburg, MD) as described by the manufacturers. PCR products were resolved on a 10% polyacrylamide gel and viewed with SYBR Green I (Molecular Probes, Eugene, OR) staining.

Colony forming efficiency (CFE) assay

The CFE assay was used as described earlier with minor modifications [13]. Heavily X-irradiated (50 Gy) IOMM-Lee cells (3.5×10^4) were used as feeder cells and were plated 24 h in advance of seeding the experimental cells. The plates were incubated for 2 weeks before the colonies were stained with methylene blue. Colonies containing at least 50 cells were counted. Plating efficiency (PE) was calculated as the ratio of the number of colonies formed to the number of cells seeded.

Quantitative PCR

Quantitative PCR was performed on cDNA templates with the I-cycler machine (Bio-Rad, Hercules, CA) and SYBR Green I (Molecular Probes, Eugene, OR) using PCR conditions and data analysis as described earlier [14]. The primers used for NF2 were 5′-ACCGTTGCC TCCTGACATAC and 5′-TCGGAGTTCTCATTG TGCAG and for hTERT were 5′-GGAAGAGTGT CTGGAGCAAG and 5′-GGATGAAGCGGAGTCTG GAC.

Immunofluorescence

Immunofluorescence was performed on meningioma cell lines for Vimentin using the clone Vim 3B4 antibody (0.5 μg/ml, Dako Corporation, Carpinteria, CA), for Desmoplakin 1 and 2 using the clone DP1-1&2-2.15 antibody (20 μg/ml, Research Diagnostics, Inc., Flanders, NJ) and for NF2 using the rabbit polyclonal NF2 (C-18) antibody (Santa Cruz Biotechnology, Inc., Santa Cruz, CA). Meningioma cell lines were grown in eight well chamber slides, fixed with 2% formaldehyde in Hanks balanced salt solution for 15 min at 37°C and permeabilized and blocked by incubation with 0.1% saponin, 10% FBS in PBS (Buffer A) for 15 min. The cells were then sequentially incubated with primary antibody and secondary antibody (4 μg/ml; Alexa Fluor 594 goat anti-mouse IgG or Alexa Fluor 488 goat anti-rabbit IgG), mounted in DAPI mounting media, examined and photographed with a Zeiss microscope.

Array CGH analysis

Genomic DNA was isolated from meningioma primary tumors or cell lines using the DNAeasy kit (Qiagen, Valencia, CA) following manufacturer's directions. Arrays spotted with 2464 mapped bacterial artificial chromosomes (BAC) covering the whole genome were hybridized with fluorescent labeled DNA, using 0.6 μg of cell line DNA and 0.8 μg of reference DNA from normal tissue [15]. The labeling reactions were performed overnight at 37 °C using Cy3-dCTP or Cy5-dCTP (Amersham Biosciences, Piscataway, NJ) and the BioPrime kit (Invitrogen, Carlsbad, CA) according to the manufacturer's instructions and unincorporated nucleotides were removed using a Sephadex G50 column (Amersham Biosciences, Piscataway, NJ). Test and reference DNAs were mixed with 100 μg of human Cot-1 DNA, ethanol precipitated, resuspended in 50 μl of hybridization solution and applied to a pre-hybridized array. Arrays were incubated at 37 °C on a slowly rocking table for approximately 72 h. Arrays were washed in 50% formamide buffer. The spotted BACs were counterstained with 4′,6′-diamino-2-phenylindole hydrochloride (DAPI). Finally, arrays were scanned and images processed by SPOT/SPROC custom software [16].

Results

Establishment of meningioma cell lines

Primary meningioma cell lines are readily cultured *in vitro*. These cell lines, however, have a limited life span usually senescing after several passages. In our laboratory, cell lines derived from Grade I meningiomas

typically senesce by population doubling 20, while cell lines derived from Grade III meningiomas senesce by population doubling 60 (data not shown). Most cancers have an activated telomere maintenance mechanism, often telomerase enzymatic activity, which is a marker of immortalization. We reasoned that meningioma cell lines undergo irreversible growth arrest because they are negative for telomerase activity and that reconstitution of this activity would immortalize meningioma cell cultures. We have derived three meningioma cell lines: SF3061-Parental, from a Grade III meningioma and SF4433-Parental and SF4068-Parental from Grade I meningiomas. All three cell lines were negative for telomerase activity, as assessed by the TRAP assay (Figure 1). IOMM-Lee, an established malignant meningioma cell line, is positive for telomerase activity.

We used retroviral–mediated gene transfer to engineer a derivative of SF3061-Parental, designated SF3061-hTERT, to express telomerase. SF3061-hTERT was positive for telomerase activity (Figure 2B). SF3061-Parental and SF3061-hTERT had an identical growth rate for 30 population doublings after which the parental cell line senesced while SF3061-hTERT continued growing with a steady population doubling time of 36 h (Figure 2C) for over 200 population doublings. Morphologically, SF3061-hTERT maintained the pattern and cytoarchitecture characteristic of the parental cell line (Figure 2A, a and b). Importantly, SF3061-hTERT formed colonies while the parental cell line did not form colonies (Figure 2D).

Next, we attempted immortalizing a Grade I meningioma derived cell line, SF4433-Parental, with telomerase. Telomerase-expressing SF4433 behaved like the parental cell line and did not grow beyond population doubling 20, suggesting that additional genetic changes are required for Grade I meningiomas to grow in culture. The human papillomavirus oncogene E6/E7 works by disrupting the retinoblastoma and the p53 pathways [17], both of which have been reported as being disrupted in malignant meningiomas [18]. We, therefore, transfected in the E6/E7 oncogenes in addition to telomerase into SF4433-Parental. The E6/E7 and telomerase expressing cell line (SF4433-E6/E7-hTERT) continued to grow in culture after the SF4433-Parental and SF4433-E6/E7 cell lines had senesced (Figure 3B). Once again, immortalized SF4433 maintained the morphology of the parental cell line (Figure 3A). SF4433-E6/E7-hTERT cells formed colonies (Figure 3C), whereas the parental cell line did not. Similar results

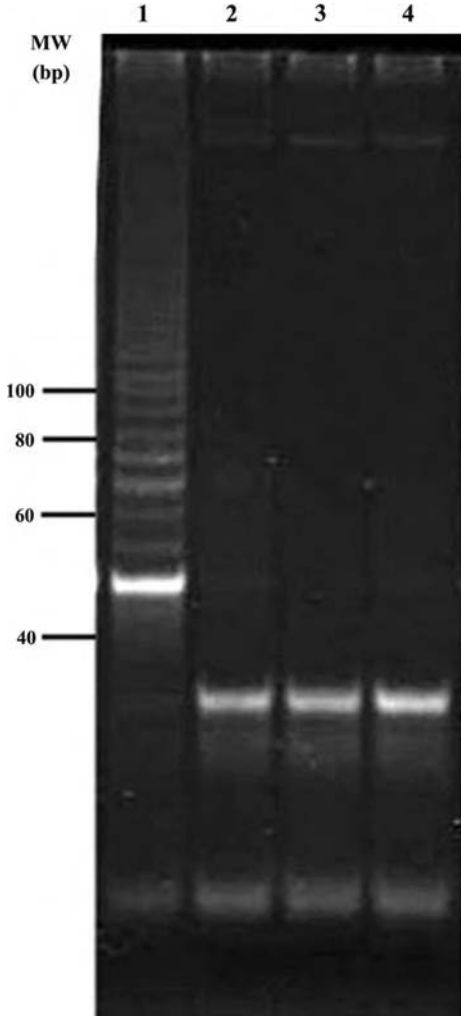

Figure 1. Meningioma cell lines, SF3061-Parental (2), SF4433-Parental (3) and SF4068-Parental (4) are negative for telomerase activity as assessed by the TRAP assay. IOMM-Lee (1), an established meningioma cell line, is telomerase positive.

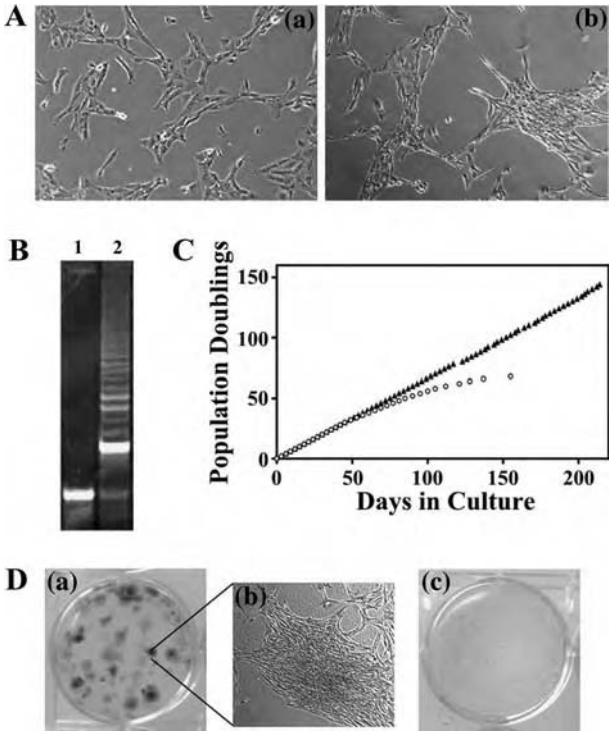

Figure 2. Expression of telomerase immortalizes SF3061-Parental, a malignant meningioma cell line. SF3061-Parental was established from a Grade III meningioma tumor and SF3061-hTERT was derived by stably expressing telomerase in SF3061-Parental. (A) The morphology of SF3061-Parental (a) is compared to SF3061-hTERT (b) at population doubling 22. Magnification is 100×. (B) Telomerase activity was measured using the TRAP assay for SF3061-Parental (1) and SF3061-hTERT (2). (C) Growth curve of SF3061-Parental (empty circles) and SF3061-hTERT (filled triangles). (D) CFE assay of SF3061-hTERT (a, b) and SF3061-Parental (c).

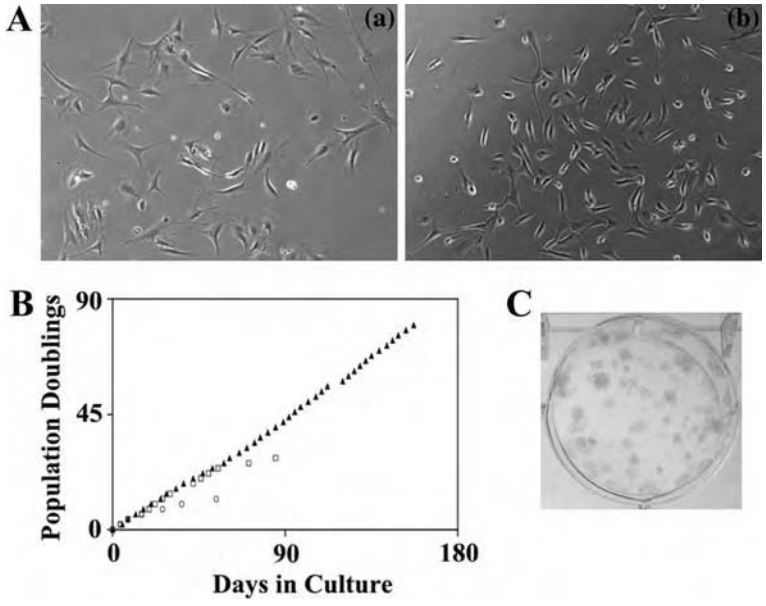

Figure 3. Immortalization of SF4433, a Grade I meningioma cell line. SF4433-Parental was established from a Grade I meningioma, SF4433-E6/E7 was derived from SF4433-Parental by stably transfecting the human papillomavirus E6/E7 oncogenes and SF4433-E6/E7-hTERT was derived by expressing telomerase in SF4433-E6/E7. (A) Morphology of SF4433-Parental (a) and SF4433-E6/E7-hTERT (b). Magnification is 100×. (B) Growth curve of SF4433-Parental (open circles), SF4433-E6/E7 (empty squares) and SF4433-E6/E7-hTERT (filled triangles). (C) CFE assay of SF4433-E6/E7-hTERT.

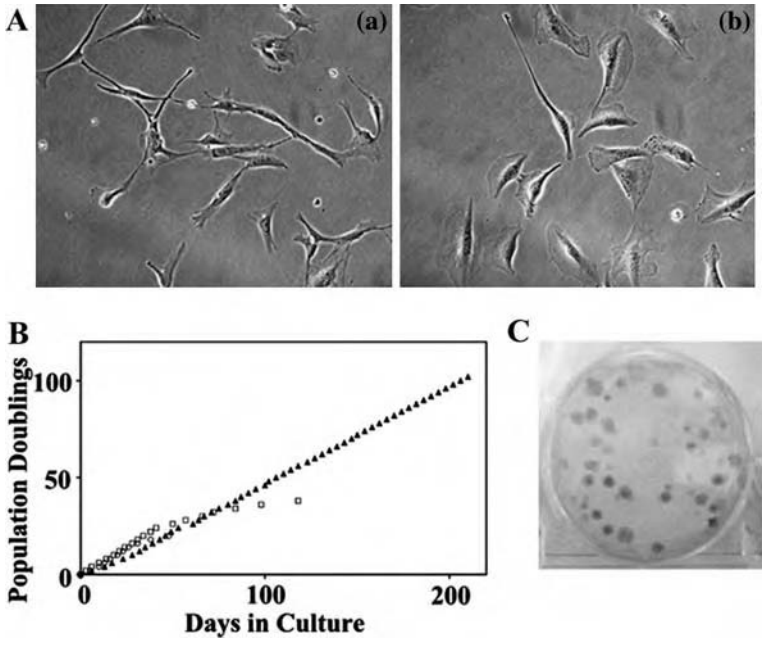

Figure 4. Immortalization of SF4068, a Grade I meningioma cell line. SF4068-Parental was established from a Grade I meningioma, SF4068-E6/E7 was derived from SF4068-Parental by stably transfecting the human papillomavirus E6/E7 oncogenes and SF4068-E6/E7-hTERT was derived by expressing telomerase in SF4068-E6/E7. (A) Morphology of SF4068-Parental (a) and SF4068-E6/E7-hTERT (b). Magnification is 200×. (B) Growth curve of SF4068-Parental (open circles), SF4068-E6/E7 (empty squares) and SF4068-E6/E7-hTERT (filled triangles). (C) CFE assay of SF4068-E6/E7-hTERT.

were obtained with SF4068, another Grade I meningioma derived cell line (Figure 4).

Primary meningioma tumors are positive for telomerase transcripts

The primary mode of repression of telomerase in human cells is through silencing of the hTERT gene via transcriptional repression [19]. Thus, quantitative PCR analysis of transcript levels is well suited to evaluate the activation status of telomerase in normal and meningioma tissues. We used this technique to assess telomerase transcript levels in the primary meningioma tumors from which the cell lines were derived. While normal meninges and brain were negative for telomerase transcripts and no PCR amplimers were observed even after 50 amplification cycles, both SF3061 and SF4433 primary tumors were positive for telomerase transcripts

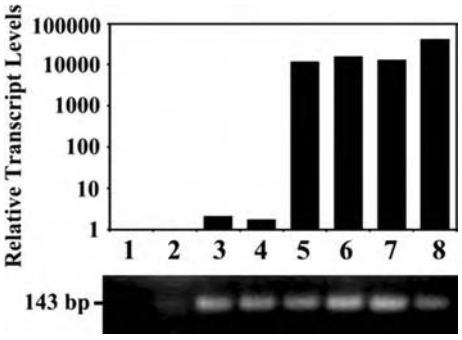

Figure 5. Telomerase expression in normal tissue, meningioma tumors and immortalized meningioma cell lines. Relative transcript levels of hTERT in non-neoplastic meninges (1), non-neoplastic brain (2), SF3061-Primary Tumor (3) SF4433-Primary Tumor (4), SF3061-hTERT (5), SF4433-E6/E7-hTERT (6), SF4068-E6/E7-hTERT (7) and IOMM-Lee (8) were compared using quantitative PCR. The corresponding 143 bp hTERT PCR amplimers after 50 PCR cycles were resolved on an agarose gel and are shown below.

(Figure 5). The telomerase transcript levels in these tumors were considerably lower that those in IOMM-Lee or in the hTERT-transduced meningioma cell lines (Figure 5).

Marker analysis of meningioma cell lines

Concomitant expression of vimentin, a class III intermediate filament protein and desmoplakin, a component of desmosomal cell junctions, is a feature unique to arachnoidal cells and meningiomas [20–22]. Using immunofluorescence, we show that SF3061-hTERT, SF4433-E6/E7-hTERT and SF4068-E6/E7-hTERT express both vimentin and desmoplakin (Figure 6), confirming that the immortalized cell lines are meningothelial in origin.

Karyotyping of meningioma cell lines

Array Comparative Genomic Hybridization (Array CGH) is a high-resolution genome-wide screening technique for the identification of amplifications and deletions of specific chromosomal regions [23, 24]. We have used this technique to karyotype the immortalized meningioma cell lines. The primary tumor from which the SF3061 cell line was derived had loss of entire chromosome 4 and 17, and losses of chromosome 9p24-p21, 11q23-qtel, 13q12-q21 (Figure 7). Interestingly, the SF3061-hTERT cell line had only a subset of the losses seen in the primary tumor (9p24-p21; 11q23-qtel; 13q12-q21; 17p). This confirmed that the cells that grew in culture bear a genomic correlation to the primary tumor. It also suggested that the SF3061 cell line was derived from a subpopulation of cells selected from the original heterogeneous tumor. We have karyotyped the commonly used IOMM-Lee cell line and compared the gross chromosomal abnormalities to that of SF3061 (Figure 7). While IOMM-Lee and the SF3061 primary tumor shared regions of loss on chromosome 4, this loss

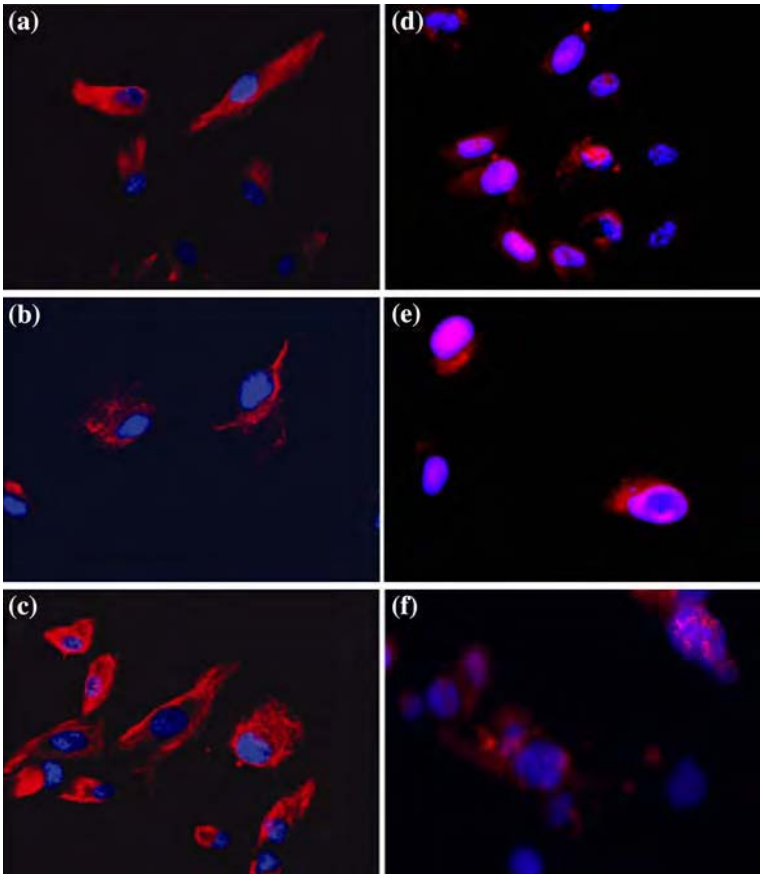

Figure 6. The meningeal origin of SF3061-hTERT (a, d), SF4433-E6/E7-hTERT (b, e) and SF4068-E6/E7-hTERT (c, f) was verified by staining for vimentin (a, b and c, red) and desmoplakin (d, e and f, red). Corresponding DAPI stains (blue) are overlaid.

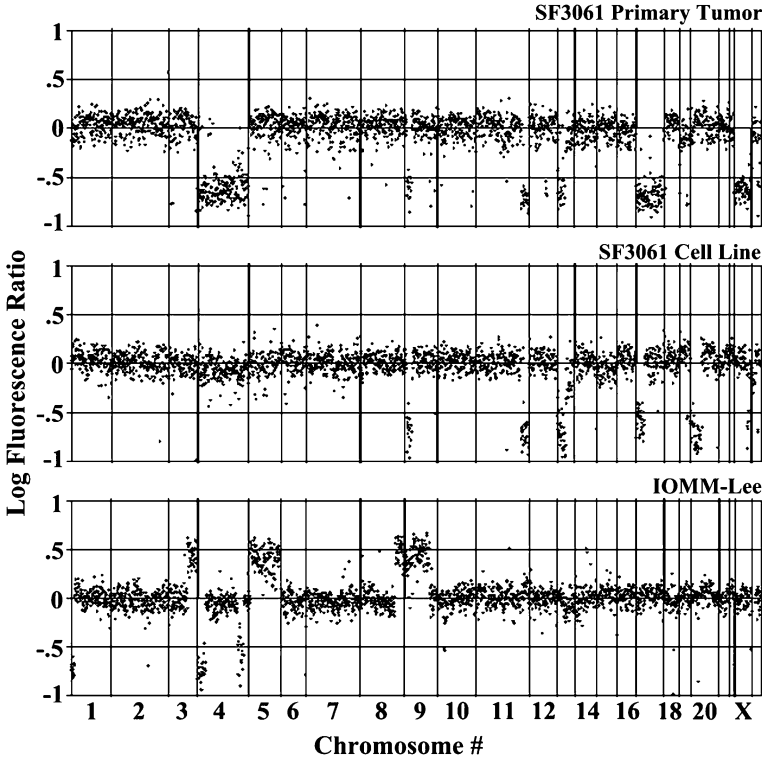

Figure 7. Karyotype of malignant meningioma cell lines. Array CGH analysis of genome copy number of SF3061 primary tumor, SF3061-hTERT cell line and the commonly used IOMM-Lee cell line are shown. The CGH ratio for each BAC array element is plotted as a function of its genome location, with chromosome 1 to the left and chromosome Y to the right, centromeric to telomeric. Vertical lines indicate chromosome boundaries.

was not conserved in the SF3061 cell line. The two cell lines had no chromosomal aberrations in common between them. IOMM-Lee had some characteristic higher-grade meningioma associated changes such as loss on 1p and gain on 9q, and SF3061-hTERT had the characteristic loss on 9p. Array CGH profiling of the Grade I primary meningioma from which SF4433 cell line was derived showed no gross chromosomal losses or gains (Figure 8). This is a phenomenon often seen in benign meningiomas (unpublished data). We have karyotyped the SF4433 cell line and found that it also had no chromosomal abnormalities. SF4068, on the other hand, had gain of chromosome 5p and loss of chromosome 15 (Figure 8). None of our three cell lines had losses on chromosome 22, a region that is often deleted in meningiomas [25].

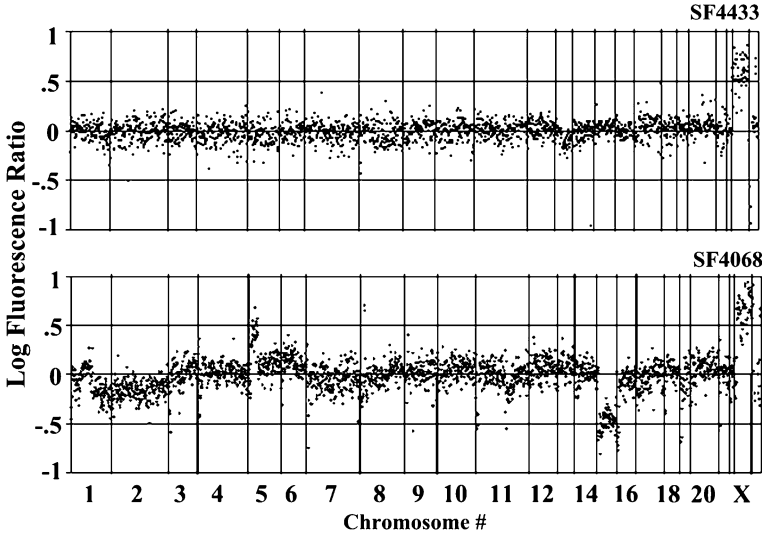

Figure 8. Karyotype of the immortalized benign meningioma cell lines. Array CGH analysis of genome copy number of SF4433 and SF4068 are shown. The CGH ratio for each BAC array element is plotted as a function of its genome location, with chromosome 1 to the left and chromosome Y to the right, centromeric to telomeric. Vertical lines indicate chromosome boundaries.

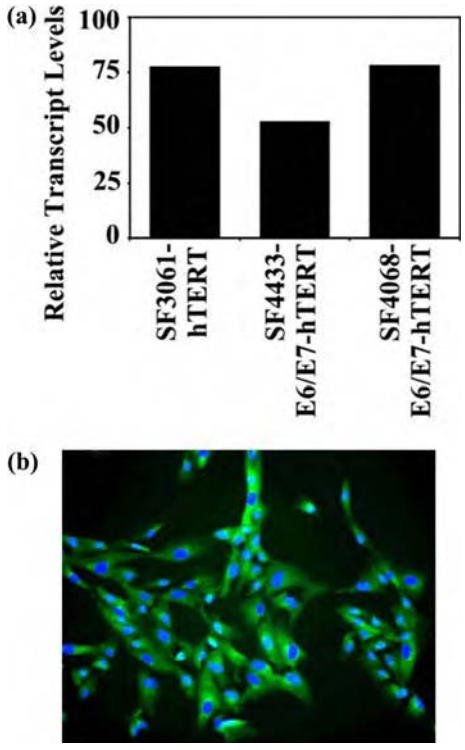

Figure 9. NF2 status of immortalized meningioma cell lines. (a) Relative transcript levels of NF2 were assessed in SF3061-hTERT, SF4433-E6/E7-hTERT, SF4068-E6/E7-hTERT using quantitative PCR. (b) Protein expression of NF2 (green) in SF3061-hTERT. Corresponding DAPI stain (blue) is overlaid.

NF2 status of meningioma cell lines

The neurofibromatosis 2 (NF2) gene located on chromosome 22 is frequently mutated in meningiomas [25]. Since we did not observe any deletions on chromosome 22 in our cell lines, we assessed the transcript and protein expression of NF2 in these cell lines. All three cell lines expressed the NF2 transcript, consistent with the observation that there were no deletions on chromosome 22 (Figure 9a). Using indirect immunofluorescence, all three cell lines were positive for the NF2 protein. A representative image of NF2 staining in SF3061-hTERT is shown in Figure 9b.

Discussion

Meningioma cell lines are notoriously resilient to growth in culture, undergoing irreversible growth arrest after a few passages *in vitro*. We have successfully produced three immortalized meningioma cell lines by inserting genetic elements that are commonly used to overcome cellular senescence and create tumor cells from normal cells [26]. Conversion of a normal human astrocyte to a human glioma requires the insertion of three key genetic elements: the expression of telomerase, functional inactivation of the p53/pRb pathways by the E6/E7 oncogenes and activation of the ras-signaling pathway by oncogenic H-ras [27]. In contrast, malignant and benign meningioma cell lines required insertion of one or two genetic changes, respectively. The other genetic change(s) are presumably inherent to the meningioma tumor from which the cell line is derived. Thus, these cell culture model systems can be used to probe the biology of meningioma tumorigenesis and are a resource critically needed by the meningioma research community.

High levels of telomerase activity and expression have been related to histological grade and tumor recurrence in primary meningioma tumors [28]. Telomerase activity and hTERT mRNA have, however, been detected in some benign meningiomas [29]. In this study, the primary tumors from which our cell lines were derived had detectable transcript levels for telomerase, suggesting that at least a subpopulation of the original tumor was telomerase positive. However, the meningioma cells that survived and grew *in vitro* were telomerase negative. The tumor microenvironment is thought to play a significant role in the activation of telomerase. hTERT expression has been reported to be regulated by hormones, growth factors, differentiation-inducing agents and other tissue-specific environmental factors [30]. It is probable that hTERT expression and activity is driven by one or more of these factors in primary meningioma tumors, and that meningioma cells, once removed from their *in vivo* environment lose expression of telomerase. It is hypothesized that primary meningioma tumors contain immortalized cells but the difficulty in obtaining cell lines is a reflection of the lack of suitable cell culture conditions.

Established cell lines from benign meningiomas without genetic manipulation do not exist. There is only one recent study that reported the successful immortalization of a benign meningioma cell line with telomerase alone [31]. This is in contrast to our results where telomerase was insufficient to immortalize two independent benign meningioma cell lines and required additional genetic changes. This is probably a reflection of particular differences in the original tumors from which these cell lines were derived. While the cell line reported in the previous study had a deletion of chromosome 22, one of our cell lines had no gross chromosomal aberrations and the other had aberrations in regions other than chromosome 22.

Overcoming the cellular senescence of benign meningioma cell lines required disruption of the p53 and pRb pathways. Both these pathways are commonly disrupted in malignant meningiomas but not in benign meningiomas. The cyclin-dependent kinase inhibitors, CDKN2A (p16) and CDKN2B (p15), regulate cell cycle progression through the G1/S-phase checkpoint, and are lost in 46–56% of Grade III meningiomas [18, 32]. This checkpoint is also under the control of phosphorylation by the retinoblastoma protein (pRB). In the p53 pathway, $p14^{ARF}$ is commonly deleted and/or mutated in malignant meningiomas [18, 32]. These genes are located on chromosome 9p, a region that is lost in the SF3061-primary tumor and cell line and consequently, SF3061 did not require disruption of these pathways for continued growth. An interesting question that arises from this study and previous observations is: What are the molecular mechanisms that allow benign meningiomas to evade cellular senescence and continue growing *in vivo*? Having access to benign meningioma cell lines

will allow meningioma researchers to begin answering this question.

The karyotypes of the three meningioma cell lines reported here are different from each other and from the established IOMM-Lee cell line. These cell lines reflect the genetic diversity seen in primary meningioma tumors. None of the cell lines reported in this study have deletions of chromosome 22 or loss of NF2, a frequent change in meningiomas. This is, however, not that surprising since approximately 40% of meningioma tumors do not have either aberrations of chromosome 22 or mutations in the NF2 gene [25, 33].

Insertion of genetic elements has undoubtedly altered some properties of the parental primary meningioma cell lines. Additionally, loss of p53 is known to enhance genomic instability [34] and it is likely that the immortalized cell lines will change characteristics over time in culture. Interpretation of results obtained using these cell lines should take these possibilities into consideration.

In conclusion, we report a genetic strategy that can be used to overcome the senescence of primary meningioma cell cultures. In addition to the cell lines reported in this study, it is anticipated that a repertoire of meningioma cell lines can be established and used to unravel the molecular basis of meningiomas.

Acknowledgements

We thank Russell O Pieper for retroviral constructs for telomerase and the human papillomavirus E6 and E7 oncogenes and the Neurological Surgery Tissue Bank at University of California, San Francisco for providing viable meningioma tumor samples. A.L. is a recipient of The Sontag Foundation Distinguished Scientist Award. This research was supported in part by The Sontag Foundation.

References

1. Lusis E, Gutmann DH: Meningioma: an update. Curr Opin Neurol 17: 687–692, 2004
2. Puduvalli VK, Li JT, Chen L, McCutcheon IE: Induction of apoptosis in primary meningioma cultures by fenretinide. Cancer Res 65: 1547–1553, 2005
3. Dirven CM, Grill J, Lamfers ML, Van der Valk P, Leonhart AM, Van Beusechem VW, Haisma HJ, Pinedo HM, Curiel DT, Vandertop WP, Gerritsen WR: Gene therapy for meningioma: improved gene delivery with targeted adenoviruses. J Neurosurg 97: 441–449, 2002
4. Ikeda K, Saeki Y, Gonzalez-Agosti C, Ramesh V, Chiocca EA: Inhibition of NF2-negative and NF2-positive primary human meningioma cell proliferation by overexpression of merlin due to vector-mediated gene transfer. J Neurosurg 91: 85–92, 1999
5. Shu J, Lee JH, Harwalkar JA, Oh-Siskovic S, Stacey DW, Golubic M: Adenovirus-mediated gene transfer of dominant negative Ha-Ras inhibits proliferation of primary meningioma cells. Neurosurgery 44: 579–587, 1999
6. Lee WH: Characterization of a newly established malignant meningioma cell line of the human brain: IOMM-Lee. Neurosurgery 27: 389–395, 1990
7. Tanaka K, Sato C, Maeda Y, Koike M, Matsutani M, Yamada K, Miyaki M: Establishment of a human malignant meningioma cell line with amplified c-myc oncogene. Cancer 64: 2243–2249, 1989
8. Sasaki M, Honda T, Yamada H, Wake N, Barrett JC, Oshimura M: Evidence for multiple pathways to cellular senescence. Cancer Res 54: 6090–6093, 1994
9. Bryan TM, Englezou A, Gupta J, Bacchetti S, Reddel RR: Telomere elongation in immortal human cells without detectable telomerase activity. EMBO J 14: 4240–4248, 1995
10. Bryan TM, Englezou A, Dalla-Pozza L, Dunham MA, Reddel RR: Evidence for an alternative mechanism for maintaining telomere length in human tumors and tumor-derived cell lines. Nat Med 3: 1271–1274, 1997
11. Campisi J: Cellular senescence as a tumor-suppressor mechanism. Trends Cell Biol 11: S27–S31, 2001
12. Kiyono T, Foster SA, Koop JI, McDougall JK, Galloway DA, Klingelhutz AJ: Both Rb/p16INK4a inactivation and telomerase activity are required to immortalize human epithelial cells. Nature 396: 84–88, 1998
13. Gupta N, Lamborn K, Deen DF: A statistical approach for analyzing clonogenic survival data. Radiat Res 145: 636–640, 1996
14. Cuevas IC, Slocum AL, Jun P, Costello JF, Bollen AW, Riggins GJ, McDermott MW, Lal A: Meningioma transcript profiles reveal deregulated notch signaling pathway. Cancer Res 65: 5070–5075, 2005
15. Snijders AM, Nowak N, Segraves R, Blackwood S, Brown N, Conroy J, Hamilton G, Hindle AK, Huey B, Kimura K, Law S, Myambo K, Palmer J, Ylstra B, Yue JP, Gray JW, Jain AN, Pinkel D, Albertson DG: Assembly of microarrays for genome-wide measurement of DNA copy number. Nat Genet 29: 263–264, 2001
16. Jain AN, Tokuyasu TA, Snijders AM, Segraves R, Albertson DG, Pinkel D: Fully automatic quantification of microarray image data. Genome Res 12: 325–332, 2002
17. Howley PM, Munger K, Romanczuk H, Scheffner M, Huibregtse JM: Cellular targets of the oncoproteins encoded by the cancer associated human papillomaviruses. Princess Takamatsu Symp 22: 239–248, 1991
18. Bostrom J, Meyer-Puttlitz B, Wolter M, Blaschke B, Weber RG, Lichter P, Ichimura K, Collins VP, Reifenberger G: Alterations of the tumor suppressor genes CDKN2A (p16(INK4a)), p14(ARF), CDKN2B (p15(INK4b)), and CDKN2C (p18(INK4c)) in atypical and anaplastic meningiomas. Am J Pathol 159: 661–669, 2001
19. Ducrest AL, Amacker M, Mathieu YD, Cuthbert AP, Trott DA, Newbold RF, Nabholz M, Lingner J: Regulation of human telomerase activity: repression by normal chromosome 3 abolishes nuclear telomerase reverse transcriptase transcripts but does not affect c-Myc activity. Cancer Res 61: 7594–7602, 2001
20. Evans RM: Vimentin: the conundrum of the intermediate filament gene family. Bioessays 20: 79–86, 1998
21. Burdett ID: Aspects of the structure and assembly of desmosomes. Micron 29: 309–328, 1998
22. Akat K, Mennel HD, Kremer P, Gassler N, Bleck CK, Kartenbeck J: Molecular characterization of desmosomes in meningiomas and arachnoidal tissue. Acta Neuropathol (Berl) 106: 337–347, 2003
23. Hodgson G, Hager JH, Volik S, Hariono S, Wernick M, Moore D, Nowak N, Albertson DG, Pinkel D, Collins C, Hanahan D, Gray JW: Genome scanning with array CGH delineates regional alterations in mouse islet carcinomas. Nat Genet 29: 459–464, 2001
24. Misra A, Pellarin M, Nigro J, Smirnov I, Moore D, Lamborn KR, Pinkel D, Albertson DG, Feuerstein BG: Array comparative genomic hybridization identifies genetic subgroups in grade 4 human astrocytoma. Clin Cancer Res 11: 2907–2918, 2005
25. De Vitis LR, Tedde A, Vitelli F, Ammannati F, Mennonna P, Bigozzi U, Montali E, Papi L: Screening for mutations in the neurofibromatosis type 2 (NF2) gene in sporadic meningiomas. Hum Genet 97: 632–637, 1996
26. Hahn WC, Counter CM, Lundberg AS, Beijersbergen RL, Brooks MW, Weinberg RA: Creation of human tumour cells with defined genetic elements. Nature 400: 464–468, 1999
27. Sonoda Y, Ozawa T, Hirose Y, Aldape KD, McMahon M, Berger MS, Pieper RO: Formation of intracranial tumors by genetically modified human astrocytes defines four pathways critical in the

development of human anaplastic astrocytoma. Cancer Res 61: 4956–4960, 2001
28. Leuraud P, Dezamis E, Aguirre-Cruz L, Taillibert S, Lejeune J, Robin E, Mokhtari K, Boch AL, Cornu P, Delattre JY, Sanson M: Prognostic value of allelic losses and telomerase activity in meningiomas. J Neurosurg 100: 303–309, 2004
29. Simon M, Park TW, Leuenroth S, Hans VH, Loning T, Schramm J: Telomerase activity and expression of the telomerase catalytic subunit, hTERT, in meningioma progression. J Neurosurg 92: 832–840, 2003
30. Ducrest AL, Szutorisz H, Lingner J, Nabholz M: Regulation of the human telomerase reverse transcriptase gene. Oncogene 21: 541–552, 2002
31. Puttmann S, Senner V, Braune S, Hillmann B, Exeler R, Rickert CH, Paulus W: Establishment of a benign meningioma cell line by hTERT-mediated immortalization. Lab Invest 85: 1163–1171, 2005
32. Simon M, Park TW, Koster G, Mahlberg R, Hackenbroch M, Bostrom J, Loning T, Schramm J: Alterations of INK4a(p16-p14ARF)/INK4b(p15) expression and telomerase activation in meningioma progression. J Neurooncol 55: 149–158, 2001
33. Carlson KM, Bruder C, Nordenskjold M, Dumanski JP: 1p and 3p deletions in meningiomas without detectable aberrations of chromosome 22 identified by comparative genomic hybridization. Genes Chromosomes Cancer 20: 419–424, 1997
34. Smith ML, Fornace AJ: Genomic instability and the role of p53 mutations in cancer cells. Curr Opin Oncol 7: 69–75, 1995

Address for offprints: Anita Lal, Brain Tumor Research Center, Department of Neurological Surgery, University of California, Box 0520 San Francisco, CA, 94143, USA; Tel.: +415-476-6662; Fax: +415-476-0388; E-mail: alal@itsa.ucsf.edu

Brain Pathology ISSN 1015-6305

RESEARCH ARTICLE

An Orthotopic Skull Base Model of Malignant Meningioma

Gilson S. Baia[1]; Eduard B. Dinca[1]; Tomoko Ozawa[1]; Edna T. Kimura[2]; Michael W. McDermott[1]; C. David James[1]; Scott R. VandenBerg[1]; Anita Lal[1]

[1] Brain Tumor Research Center, Department of Neurological Surgery, University of California, San Francisco, CA 94143.
[2] Department of Cell and Developmental Biology, Institute of Biomedical Sciences, University of Sao Paulo, Sao Paulo, SP, Brazil.

Keywords
bioluminescent imaging, IOMM-Lee, meningioma, orthotopic, skull base, xenografts.

Corresponding author:
Anita Lal, PhD, Brain Tumor Research Center, Department of Neurological Surgery, Box 0520, University of California, San Francisco, CA 94143 (E-mail: *anita.lal@ucsf.edu*)

Received: 23 May 2007; revised 27 July 2007; accepted 4 September 2007.

doi:10.1111/j.1750-3639.2007.00109.x

Abstract

Meningioma tumor growth involves the subarachnoid space that contains the cerebrospinal fluid. Modeling tumor growth in this microenvironment has been associated with widespread leptomeningeal dissemination, which is uncharacteristic of human meningiomas. Consequently, survival times and tumor properties are varied, limiting their utility in testing experimental therapies. We report the development and characterization of a reproducible orthotopic skull-base meningioma model in athymic mice using the IOMM-Lee cell line. Localized tumor growth was obtained by using optimal cell densities and matrigel as the implantation medium. Survival times were within a narrow range of 17–21 days. The xenografts grew locally compressing surrounding brain tissue. These tumors had histopathologic characteristics of anaplastic meningiomas including high cellularity, nuclear pleomorphism, cellular pattern loss, necrosis and conspicuous mitosis. Similar to human meningiomas, considerable invasion of the dura and skull and some invasion of adjacent brain along perivascular tracts were observed. The pattern of hypoxia was also similar to human malignant meningiomas. We use bioluminescent imaging to non-invasively monitor the growth of the xenografts and determine the survival benefit from temozolomide treatment. Thus, we describe a malignant meningioma model system that will be useful for investigating the biology of meningiomas and for preclinical assessment of therapeutic agents.

INTRODUCTION

Meningiomas are common tumors of the central nervous system that originate from the meningeal covering (22), and therefore can occur in any location along the entire neural axis. They are a source of considerable morbidity and mortality because of their location and the existence of aggressive variants (18). Nevertheless, meningiomas remain a poorly understood cancer. A major obstacle to achieving an improved understanding of the molecular basis of meningioma tumorigenesis, and to evaluating experimental therapies for meningioma treatment, has been the scarcity of *in vitro* and *in vivo* model systems. Recently, considerable progress has been made in successfully growing meningioma cell lines *in vitro* (1, 20). These cell lines represent promising new tools for investigating the biology of meningiomas. However, *in vivo* meningioma model systems still have problems that restrict their utility (11, 16, 27).

Attempts at propagating available meningioma cell lines as orthotopic xenografts have been unable to recapitulate the human tumor growth pattern, as implantation of tumor cells results in widespread leptomeningeal dissemination throughout the subdural and intraventricular space (16, 27). Consequently, quantification of tumor growth as well as response to therapeutic agents is difficult compromising the utility of the model systems (16). The purpose of this study was to locally constrain meningioma tumor growth and develop a clinically relevant meningioma model system in athymic mice. Because skull base meningiomas are challenging to remove surgically and patients with these meningiomas have a worse prognosis (15, 17), we chose to develop a skull base model using the malignant meningioma cell line, IOMM-Lee, which is tumorigenic *in vivo* and grows at a rapid rate (13). By modifying these cells with a luciferase reporter, we have been able to additionally use bioluminescent imaging (BLI) to monitor *in vivo* growth of these cells, as well as their response to temozolomide therapy.

MATERIALS AND METHODS

Generation of enhanced green fluorescent protein and firefly luciferase expressing IOMM-Lee cells

The intraosseous malignant meningioma derived cell line, IOMM-Lee, was used in all the experiments described in this report (13, 14). IOMM-Lee cells were electroporated (Gene Pulser X Cell, Biorad, Hercules, CA, USA) with the enhanced green fluorescent protein (EGFP)-N3 plasmid (BD Biosciences, San Jose, CA, USA) and single clones expressing EGFP were selected in 600 μg/mL G418. IOMM-Lee cells were tagged with firefly luciferase (fluc) under the control of the spleen focus forming virus promoter using lentiviral-mediated gene transfer (9). Lentiviruses were generated

by cotransfection of 293T cells with plasmids for gag-pol, env and fluc. The 48 h post-transfection filtered supernatant was used to infect IOMM-Lee cells.

Intracranial IOMM-Lee transplantations

All animal experiments were conducted following protocols approved by the University of California, San Francisco, Institutional Animal Care and Use Committee. Five- to six-week-old female athymic mice were anesthetized with Ketamine/Xylazine and fixed in a Model 940 stereotactic frame (David Kopf Instruments, Tujunga, CA, USA). The skull base region was reached by using the following injection coordinates: 2 mm to the right of the bregma, 2 mm posterior to the bregma and 5.8 mm below the skull surface. The indicated cell numbers and volumes of IOMM-Lee suspended in phosphate buffered saline (PBS) or matrigel were implanted using a Model 5000 Microinjection Unit (David Kopf Instruments, Tujunga, CA, USA) loaded with a 5 μL Hamilton 7105 syringe. For injection volumes of 0.5 μL, cells were steadily implanted over a period of 70 s and the needle was left in place for 1 minute before it was withdrawn slowly. The skull burr-hole was sealed with bone-wax and the skin incision was closed with 7 mm staples. Control mice were implanted with matrigel alone. The mice were monitored closely and were euthanized if they exhibited any neurological symptoms or had >15% weight loss or at predefined times post-implantation. The estimated survival times were the times from cell implantation to euthanasia.

Tissue processing and immunohistochemistry

EGFP fluorescence in tumor cells was analyzed in formalin fixed mouse heads after removal of the skull with a Leica MZ Fluo III stereomicroscope equipped with a Leica GFP-plus filter set. For histopathologic examination, mouse heads with the skull intact were fixed in 10% neutral buffered formalin for 48 h, decalcified in Decal Rapid Bone Decalcifier (American Histology, Lodi, CA, USA) for 24 h, and embedded in paraffin. Serial 10 μm thick sections were cut, numbered and processed for either hematoxylin and eosin (H&E) staining or immunohistochemistry. Immunohistochemistry was performed for vimentin using the clone Vim 3B4 antibody (1:100; Dako Corporation, Carpinteria, CA, USA), for carbonic anhydrase 9 (CA9) using the NB 100-417 antibody (1:1000; Novus Biologicals, Littleton, CO, USA) and for the Ki67 antigen using the clone MIB-1 antibody (1:100; Dako Corporation, Carpinteria, CA, USA) as described earlier (28). For calculating the MIB-labeling index, a total of 1000 nuclei in three hot-spots were counted.

BLI of luciferase—IOMM-Lee xenografts

BLI of intracranial xenografts was performed using the IVIS Lumina System (Xenogen Corp., Alameda, CA, USA) coupled to the data-acquisition LivingImage software (Xenogen Corp.). Before imaging, the mice were anesthetized with Ketamine/Xylazine. Thirty mg/mL of luciferin (potassium salt; Gold Biotechnology, St Louis, MO, USA) in PBS was injected intraperitoneally at a dose of 150 mg/kg body weight. Images were acquired between 10 and 20 minutes post-luciferin administration and peak luminescent signal was recorded. Signal intensity was quantitated as the sum of all detected photon counts within a region of interest using the LivingImage software package (6).

Temozolomide treatment and statistical analysis

For assaying *in vitro* sensitivity to temozolomide (TMZ), 100 000 IOMM-Lee and IOMM-Lee-Luc cells were plated in six well plates and the indicated concentration of TMZ was added at 24, 48 and 72 h. At 144 h, the cells were trypsinized, resuspended in 1 mL media and processed using the MTT Cell Proliferation Assay (ATCC, Manassas, VA, USA) following manufacturer's direction. Absorbance was read at 590 nm. The luminescence of IOMM-Lee-Luc cells treated with TMZ as described above was also read at 144 h in six well plates using the IVIS Lumina System in the presence of 30 μL of 30 mg/mL luciferin (potassium salt; Gold Biotechnology, St Louis, MO, USA). All *in vitro* experiments were performed in triplicate. For assaying *in vivo* sensitivity to TMZ, five mice bearing IOMM-Lee xenografts were orally administered with 120 mg/kg of TMZ for four consecutive days starting on day 10. Five mice bearing IOMM-Lee xenografts constituted the control group and received no treatment. The Kaplan-Meier estimator was used to generate the survival curves (12). Differences between survival curves were compared using a log-rank test (19).

Methylation-specific polymerase chain reaction (MSP)

Genomic DNA from IOMM-Lee cells was isolated using the DNeasy kit (Qiagen, Valencia, CA, USA). The methylation status of the O^6-methylguanine-DNA methyltransferase (MGMT) gene promoter was determined by MSP as described earlier (4, 7). Bisulfite treatment of isolated DNA was performed using the EZ DNA Methylation Gold kit (Zymo Research, Orange, CA, USA), followed by polymerase chain reaction (PCR) amplification to distinguish methylated and unmethylated DNA using PCR conditions and primers described earlier (7).

RESULTS

Fluorescent and bioluminescent tagging of IOMM-Lee cells

In order to accurately assess the extent of leptomeningeal dissemination, IOMM-Lee cells were fluorescently labeled with EGFP and a single high-level EGFP expressing clone, designated IOMM-Lee-EGFP2, was selected for further analysis. For BLI, IOMM-Lee cells were transduced with lentivirus encoding firefly luciferase, and transduced cell pools (IOMM-Lee-Luc) were injected in mice. IOMM-Lee-EGFP2, IOMM-Lee-Luc and parental IOMM-Lee had similar growth curves *in vitro* (data not shown). Also, IOMM-Lee-EGFP2 and parental IOMM-Lee had similar growth curves as subcutaneous tumors in athymic mice (data not shown). Thus, there was no indication of fluorescent and bioluminescent labeling altering the growth properties of IOMM-Lee parental cells.

Estimated survival times

We injected varying amounts and concentrations of IOMM-Lee-EGFP2 cells in PBS or matrigel into the skull base region of

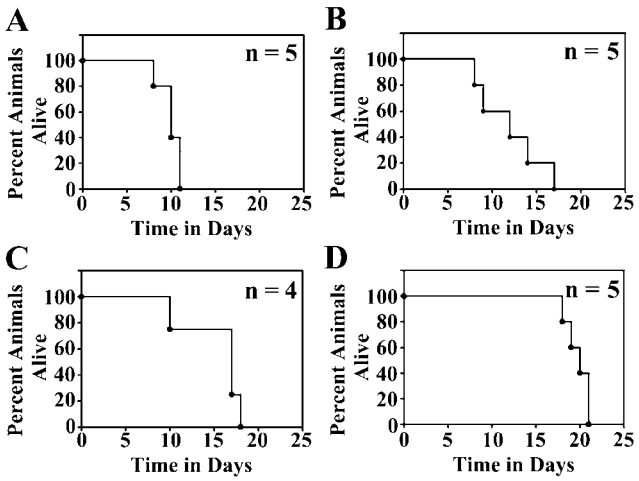

Figure 1. Estimated survival curves of athymic mice implanted with IOMM-Lee-EGFP2 cells in the skull base region. Athymic mice implanted with 3 000 000 cells/3 µL (**A**), 500 000 cells/5 µL (**B**), 50 000 cells/1 µL (**C**) or 50 000 cells/0.5 µL (**D**) were euthanized when they exhibited neurological symptoms or weight loss. Kaplan Meier plots for each implantation condition and the numbers of mice (n) in each group are shown.

athymic mice and calculated estimated survival times based on the appearance of neurological symptoms or weight loss. All the mice injected with IOMM-Lee-EGFP2 cells developed tumors. Thus, the tumor take rate with this cell line is 100%. Considerable variability in survival times and widespread leptomeningeal dissemination throughout the skull base and subarachnoid space was observed when PBS was used as an implantation medium (data not shown). When matrigel was used as an implantation medium, both intra- and inter-group variability in survival times were observed, with the extent of the former depending on both cell number and cell volume injected (Figure 1). For example, mice injected with 500 000 cells/5.0 µL died as early as 8 days or as late as 17 days (Figure 1), and this variability was caused by differences in tumor cell dissemination between mice receiving this amount and concentration of cells (data not shown). More consistent survival times with mice dying within 5 days of each other was observed for injections of 3 million cells/3.0 µL and 50 000 cells/0.5 µL (Figure 1). Of these two conditions, mice injected using the latter condition had slightly longer estimated survival times of 17–21 days and were chosen for use in subsequent investigations (see below).

Localized meningioma tumor growth

Macroscopic analysis of IOMM-Lee-EGFP2 xenograft growth revealed that the tumor mass did not invade the surface of the brain, and typically adhered to periosteal membranes when the skull and brain were separated (Figure 2). Examination of EGFP fluorescence revealed that tumor growth was confined to the site of implantation with minimal tumor cell dissemination to surrounding locations (Figure 2). The brain was visibly compressed at the location of the tumor.

Histopathology of IOMM-Lee xenografts

Histopathologic analyses were performed on tumors that were fixed, processed and sectioned *in situ* with the skull and brain intact. Xenografts displayed histopathologic features that were reminiscent of human anaplastic meningiomas, and included high cellularity, prominent nuclear pleomorphism marked by a high

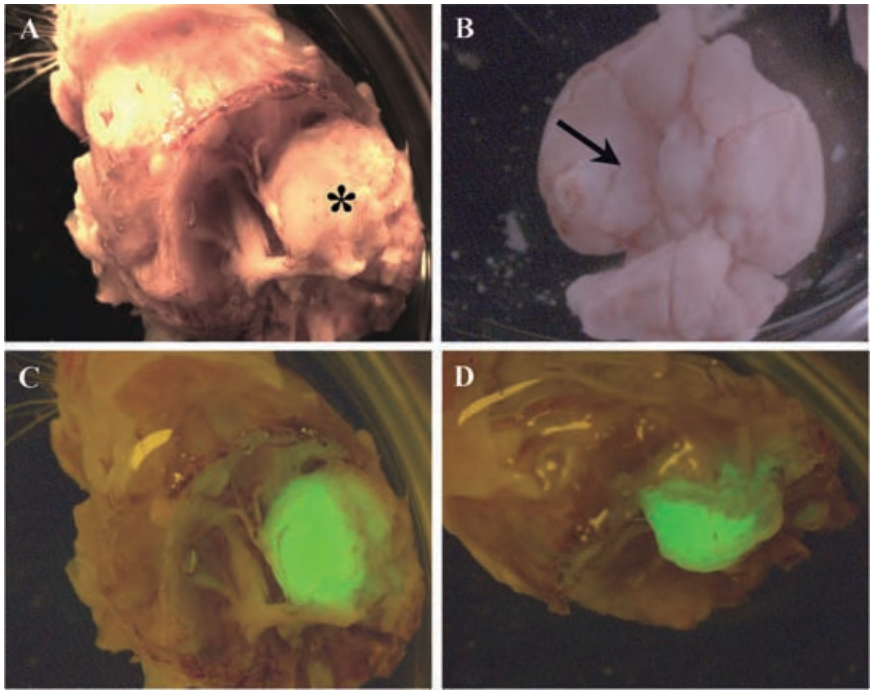

Figure 2. Macroscopic view of IOMM-Lee skull base meningioma xenografts. IOMM-Lee-EGFP2 cells were implanted in the skull base region using matrigel as the implantation medium to obtain localized tumor growth. The tumor mass (asterisk in **A**) was observed between the brain and the skull, and adhered to the skull when the skull (**A**) and brain (**B**) were separated. Compression of the brain was observed (arrow in **B**). Minimal leptomeningeal dissemination was observed as assessed by the distribution of the fluorescent EGFP label (**C**,**D**).

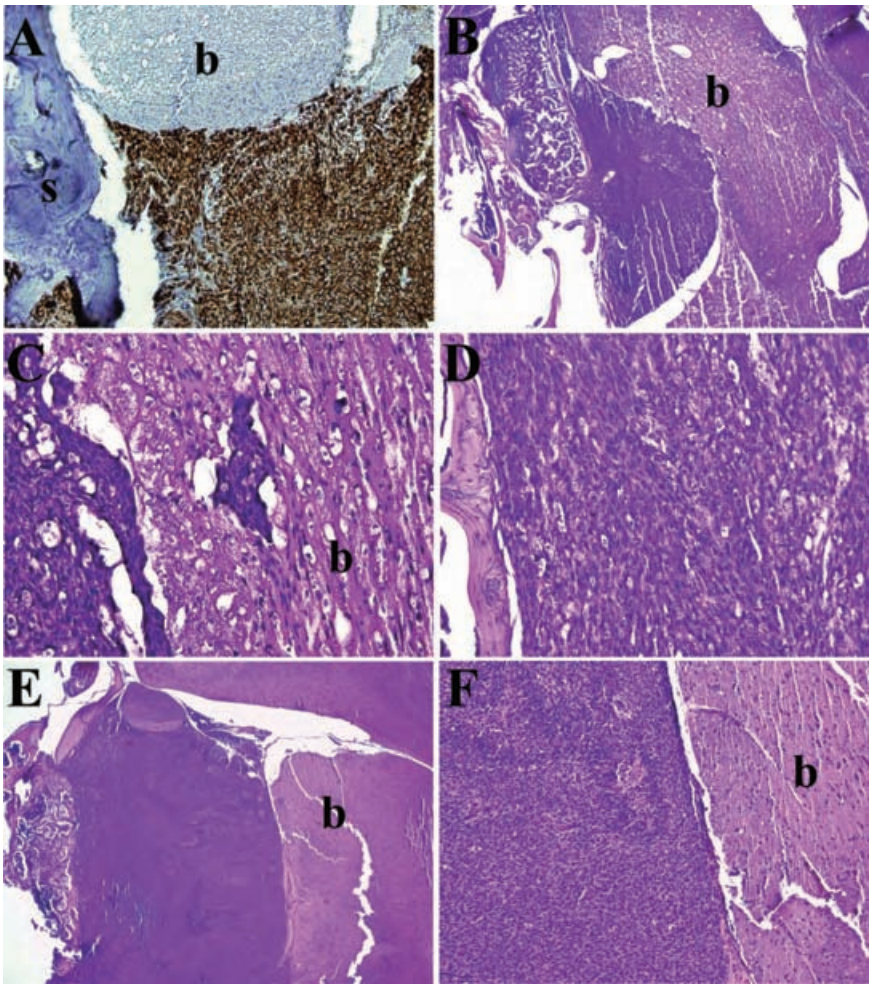

Figure 3. Growth Characteristics of IOMM-Lee skull base xenografts. Tissue sections of IOMM-Lee xenografts on day 6 (**A**), day 9 (**B**–**D**) and day 12 (**E**,**F**) were stained with human vimentin (**A**) or hematoxylin and eosin (**B–F**) and examined to evaluate the pattern of tumor growth. IOMM-Lee tumor growth maintained a well-demarcated boundary with the brain, except for microinvasion of the brain by small clumps of tumor cells (**C**). s, skull; b, brain.

nuclear to cytoplasmic ratio and prominent nucleoli. Cells were typically arranged in syncytial-like, highly cellular sheets with variable amounts of micro and geographic necrosis. Mitotic figures were conspicuous and the MIB-1 labeling indices were typically 30%.

Growth characteristics of IOMM-Lee xenografts

To evaluate xenograft growth patterns, brains with intact skulls were resected from mice injected with IOMM-Lee-Luc cells (50 000/0.5 μL) and sacrificed at days 3, 6, 9, 12, 16 post-implantation or when they exhibited weight loss and/or neurological symptoms. Fixed and embedded brain and skull tissue was serially sectioned, and examined by conventional H&E analysis or after staining for human vimentin. Progressive tumor growth was evident from day 3 onward, and by day 6, the tumor appeared to erode into the adjacent skull while primarily compressing the brain with early multifocal invasion into perivascular spaces (Figure 3). As the tumor mass enlarged, the boundary with the brain remained well-demarcated except for regions of microinvasion (Figures 3 and 4). By day 12 the xenografts had conspicuous necrotic zones, and the tumors had breached the pia and were invading the brain along perivascular and cranial nerve tracts (Figure 4). Immunohistochemical staining for human vimentin gave no indication of tumor dissemination at locations distant from the site of tumor implantation, and therefore meningioma tumor growth was localized to the site of tumor implantation.

Tumor hypoxia is an endogenous characteristic of malignant meningiomas, is associated with higher-grade histology as well as aggressive clinical behavior (28). With respect to this animal model of malignant meningioma, we assessed the appearance and prevalence of hypoxia by CA9 immunohistochemistry (28). Regions of hypoxia were first visible in day 9 xenografts (Figure 5), prior to the appearance of necrosis. Extensive hypoxic cell numbers were observed at the brain interface suggesting that this edge of the tumor was slower at recruiting vessels from the neuropil as opposed to non-brain interface tissue. Necrosis was first observed in day 12 tumors (Figure 5), and similar to human meningiomas, CA9 staining was zonal, found in viable cells surrounding regions of necrosis and also in regions not associated with any visible necrosis.

BLI of meningioma tumor burden

BLI was used to quantitate intracranial meningioma tumor growth rates in advance of testing tumor response to alkylator therapy.

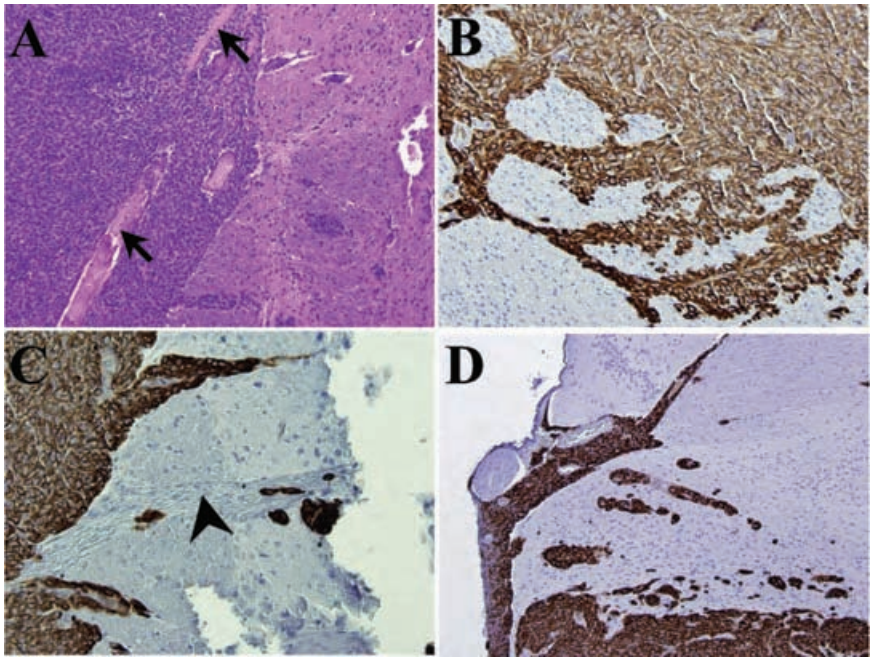

Figure 4. Pattern of brain invasion by IOMM-Lee xenografts. Tissue sections of IOMM-Lee xenografts on day 12 (**A–C**) or day 16 (**D**) were stained with human vimentin (**B–D**) or hematoxylin and eosin (**A**) and examined to evaluate the pattern of invasion of brain. By day 12, the tumor had breached the pia (**A**) and was invading the brain along perivascular (B) and cranial nerve (**C**) tracts. A similar pattern of invasion was observed in day 16 tumors (**D**). Arrow, pia; arrowhead, cranial nerve.

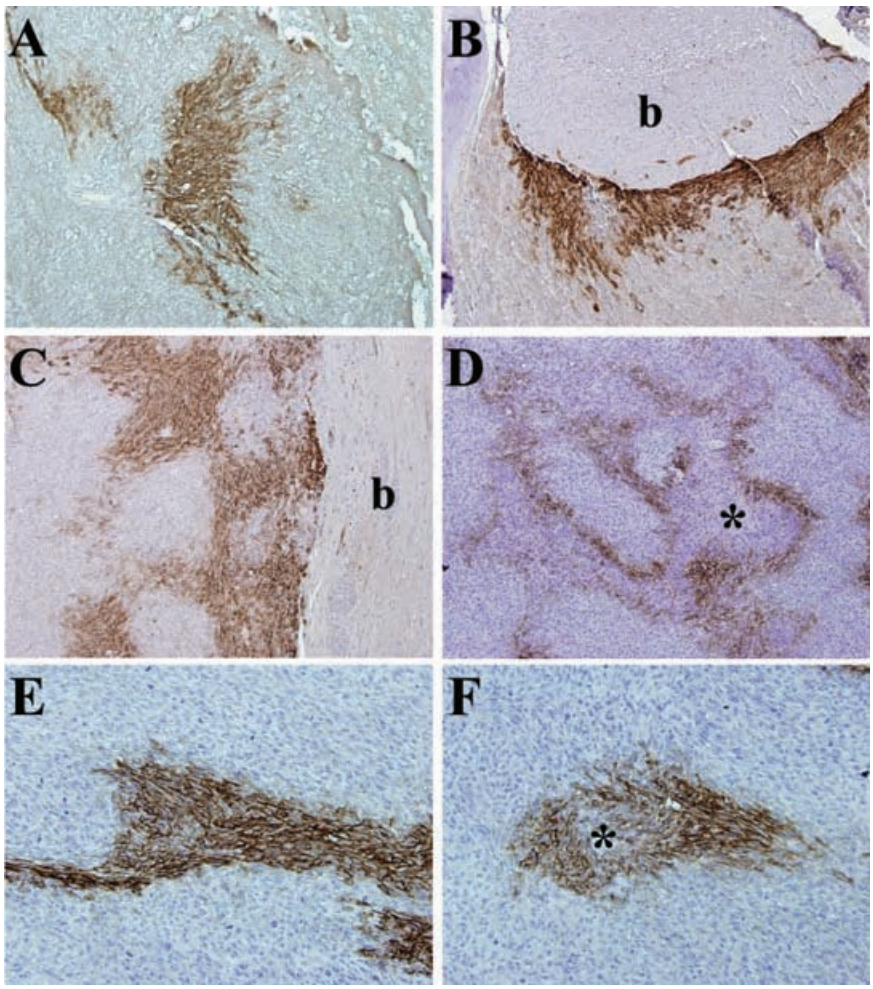

Figure 5. Pattern of hypoxia in IOMM-Lee skull-base xenografts. Immunohistochemistry with a polyclonal antibody against carbonic anhydrase 9 (CA9) was performed to evaluate the prevalence and distribution of hypoxia in tissue sections of IOMM-Lee xenografts on day 9 (**A**), day 12 (**B**), day 16 (**C**) and day 21 (**D–F**) post-implantation. Similar to human meningiomas, CA9 expression was zonal and sometimes not associated with any visible necrosis (**E**). The brain interface had considerable hypoxia (**B**,**C**) compared with the skull interface. b, brain; *, necrosis.

Luminescence readings were detectable as early as day 3, and growth curves displayed consistent patterns of exponential increase between mice. Mice exhibited weight loss and neurological symptoms when photon counts of $3–4 \times 10^7$ were reached. In total, the BLI results showed reproducible growth of skull base xenografts, and provided pilot data for use in timing the administration of therapy in the subsequent experiment.

Xenograft response to TMZ therapy

To assess the efficacy of alkylator therapy, we treated IOMM-Lee and IOMM-Lee-Luc cells in culture with TMZ (Figure 6A,B). IOMM-Lee was sensitive to TMZ *in vitro* and the bioluminescent labeling did not alter the sensitivity to TMZ. Sensitivity to TMZ has been associated with *MGMT* promoter hypermethylation, and the *MGMT* promoter was methylated in IOMM-Lee cells (Figure 6C). To assess the *in vivo* sensitivity of IOMM-Lee xenografts to TMZ, tumor growth in control and TMZ-treated mice were followed using BLI. TMZ treatment resulted in a significant survival benefit to the mice (Figure 6, $P = 0.003$). While control group mice died by 17–21 days, one TMZ-treated mouse died on day 38 and the remaining four were still alive on day 43. To plot BLI tumor growth curves, each mouse's luminescence measurements were normalized against their own day 10 luminescence reading, allowing each mouse to serve as its own control. TMZ treatment arrested the rapid, exponential growth of the xenografts and resulted in reduced normalized luminescence readings (Figure 7). Recovery of exponential tumor growth was observed in the TMZ-treated mouse that died on day 38, while the remaining four mice had stable luminescent measurements till day 43 (Figure 7).

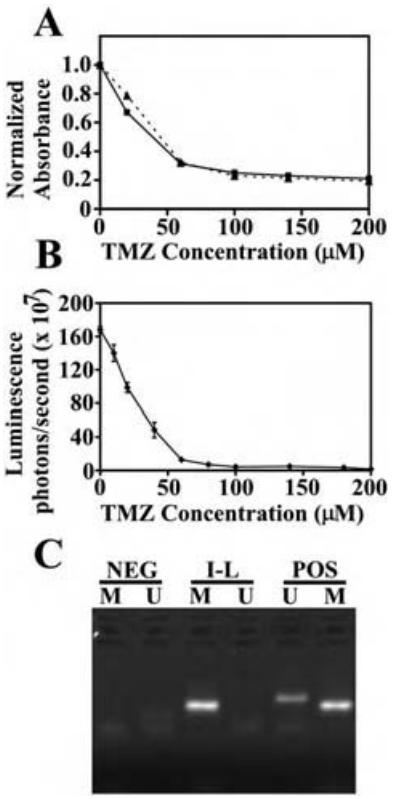

Figure 6. Efficacy of temozolomide (TMZ) in cultured IOMM-Lee cells and methylation status of the *O⁶-methylguanine-DNA methyltransferase (MGMT)* promoter. **A.** IOMM-Lee (squares and solid line) or IOMM-Lee-Luc cells (triangles and dashed line) were treated with the indicated concentration of TMZ and the number of viable cells was calculated using the MTT Cell Proliferation assay. Absorbance values were normalized to the no treatment control and plotted against TMZ concentration. The number of viable cells at different TMZ concentrations was similar for IOMM-Lee and IOMM-Lee-Luc cells. **B.** IOMM-Lee-Luc cells in culture were treated with the indicated concentration of TMZ and luminescence was measured at 144 h. Luminescence readings are plotted against TMZ concentration. **C.** Methylation-specific polymerase chain reaction was performed to determine the methylation status of the *MGMT* gene. The presence of a visible polymerase chain reaction product in the lane U indicates the presence of unmethylated *MGMT* gene and the presence of product in the lane M indicates the presence of methylated *MGMT* gene. *MGMT* is methylated in IOMM-Lee. Abbreviations: NEG = negative controls; I-L = IOMM-Lee; POS = positive controls.

DISCUSSION

Animal models are essential preclinical tools in the study of the molecular mechanisms of cancer and for evaluating anti-tumor therapies. A small number of meningioma animal models exist but every one of these systems has issues that limit their utility and/or clinical relevance. For example, in the genetic model of meningiomas, which is based on the knockout of the *NF2* gene specifically in arachnoidal cells, only 20% of the mice develop tumors after 11 to 14 months (11). Other model systems have utilized non-orthotopic locations that do not take micro-environmental influences of tumor growth into consideration. Rodent studies on the chemotherapeutic agent, hydroxyurea, were performed using meningioma cells grown in the galea (25), and tests on celecoxib were performed in subcutaneous tumors (21). Orthotopic meningioma model systems utilizing primary and established meningioma cell lines have been described (16, 27). However, primary meningioma cell lines senesce after a few passages and therefore these model systems are not reproducible (16, 27). Orthotopic models with established meningioma cell lines have been associated with widespread leptomeningeal dissemination limiting the ability to quantitate the extent of tumor growth in these systems.

In this study, we present a well-characterized, reproducible, clinically relevant skull base malignant meningioma xenograft model system in which we have overcome the problem of leptomeningeal dissemination. We show that localized meningioma tumor growth is sensitive to particular cell densities and is dependent on using matrigel as the implantation agent. In addition, we show that mice bearing localized xenografts had reproducible survival times within a range of 5 days. IOMM-Lee has been extensively used in meningioma research (23, 26) and has previously been implanted into the skull base region of mice (16, 27). However, localized tumor growth using this cell line has not previously been attained. Prior studies utilized PBS as the implantation agent, and it is likely that the use of matrigel would have reduced observed tumor cell dissemination. Previous reports of survival times with mice bearing IOMM-Lee orthotopic xenografts were similar to the survival times in this study (16, 24).

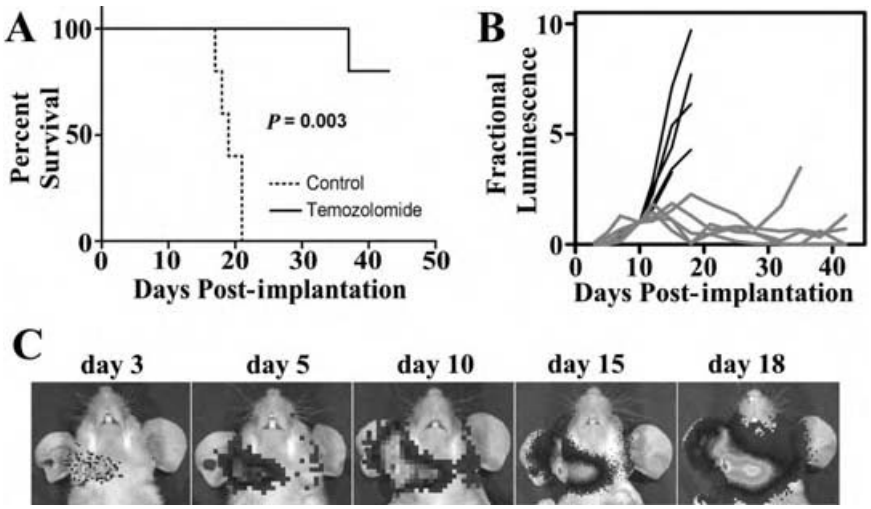

Figure 7. Bioluminescent imaging of IOMM-Lee xenografts, and their response to temozolomide (TMZ). Ten mice received injections of IOMM-Lee-Luc cells and were randomized into two groups that received either no treatment or treatment with 120 mg/kg TMZ for four consecutive days. **A.** Survival curves of athymic mice from control (dotted line) and TMZ-treatment (solid line) groups are plotted. A significant survival benefit ($P = 0.003$) for mice treated with TMZ was observed. **B.** Luminescence readings for each mouse were normalized against its own day 10 luminescence reading. Normalized BLI plots associated with monitoring of intracranial tumor growth for control (black line) and TMZ-treatment (gray line) groups are shown. **C.** Representative images from one control group mouse at the indicated time points post-implantation of IOMM-Lee-Luc cells are shown.

Preclinical cancer models should ideally resemble the human disease and mimic human tumor-host interactions. Human meningiomas are generally well-demarcated lesions that remain spherical or globular even after they attain considerable size (3). Consistent with the growth pattern of human meningiomas, IOMM-Lee xenografts grew as well-demarcated lesions between the skull and brain and remained globular even when the tumor mass was large. Malignant meningiomas commonly penetrate dura and invade bone. IOMM-Lee xenografts adhere to the skull and exhibit considerable invasion of the skull. Considerable compression of the brain was also observed. Human meningiomas grow as separate entities adjacent to the brain but often insinuate themselves into the subjacent cortex as small tongues or pegs of neoplastic tissue that follow the course of superficial blood vessels (3). IOMM-Lee xenografts followed a similar pattern of brain invasion, with small cell clumps invading the surrounding brain along perivascular and cranial nerve tracts.

Tumor hypoxia is significantly associated with higher histopathologic grade in meningiomas and is indicative of an aggressive meningioma phenotype (28). Similar to human meningiomas, the pattern of hypoxia in IOMM-Lee xenografts was found in the classic perinecrotic pattern in larger tumors with visible necrosis. Additionally, as in human meningiomas, hypoxia was found in histologically viable regions of tumors not associated with any visible necrosis. Interestingly, the amount of hypoxia at the brain interface was considerably greater than that at the skull interface, suggesting that the skull interface had easier access to a vascular supply. While the contribution of tumor hypoxia to meningioma growth is unknown, the current model system will allow such investigations and also allow testing of therapeutic strategies that target both normoxic and hypoxic cells.

BLI is an extremely accurate predictor of intracranial tumor burden and it has recently been shown using intracranial glioblastoma xenografts that there is an excellent correlation between intracranial tumor photon emission and tumor volume (6). BLI tumor growth curves for the IOMM-Lee xenografts were consistent between mice and BLI could accurately predict survival. Thus, BLI is ideal for following intracranial meningioma tumor growth and for monitoring therapeutic response. Meningioma tumor growth in animals has previously been monitored using contrast enhanced magnetic resonance imaging (MRI) (27). While MRI accurately follows tumor growth, it is a less cost–effective technique and relatively few researchers have access to such a facility. Immortalized benign meningioma cell lines have recently been developed in several laboratories (5, 20). These cell lines grow very slowly in mice and require long *in vivo* observation periods of several months. It is anticipated that BLI will be especially useful in following the tumor growth and monitoring the therapeutic response of these slower growing but more common meningiomas.

TMZ, a DNA methylating agent, has schedule-dependent antitumor activity against a variety of malignancies, including gliomas and melanomas (8). Currently, it is routinely used in the clinic to treat malignant gliomas. The efficacy of TMZ against malignant meningiomas has not been evaluated. In the current study, we show that TMZ was an effective therapy against rodent IOMM-Lee xenografts and resulted in a considerable survival benefit. Methylation of the promoter of the DNA-repair gene, *MGMT*, has been associated with sensitivity to TMZ in glioblastoma patients (10). The *MGMT* promoter was methylated in IOMM-Lee cells. Sixteen percent of all meningiomas have aberrant methylation of the *MGMT* promoter (2) and patients bearing these tumors could possibly respond to TMZ therapy. However, more detailed preclinical

studies using this chemotherapeutic agent are necessary before conclusions on the effectiveness of TMZ as a therapeutic agent for meningiomas are made.

In summary, we have developed a rodent preclinical meningioma model system and show that it can be used to evaluate therapeutic regimens. This system has several features that mimic the human meningioma growth pattern and will enable us to dissect the biology of meningioma tumorigenesis, evaluate tumor-host interactions unique to meningiomas and test the toxicity and efficacy of novel therapeutic approaches.

ACKNOWLEDGMENTS

We thank Cynthia Cowdrey for technical assistance with tissue processing, Lily Hu for technical assistance with generation of the luciferase lentivirus, Jennifer Ayers-Ringler for technical assistance with the *MGMT* promoter methylation assay and Drs Katharine Striedinger and Jeanette Hyer for useful discussions and review of the manuscript. This study was supported by NIH/NINDS grant 1R03NS054829-01 to AL and SPORE grant P50CA097257 to CDJ.

REFERENCES

1. Baia GS, Slocum AL, Hyer JD, Misra A, Sehati N, Vandenberg SR *et al* (2006) A genetic strategy to overcome the senescence of primary meningioma cell cultures. *J Neurooncol* **78**:113–121.
2. Bello MJ, Aminoso C, Lopez-Marin I, Arjona D, Gonzalez-Gomez P, Alonso ME *et al* (2004) DNA methylation of multiple promoter-associated CpG islands in meningiomas: relationship with the allelic status at 1p and 22q. *Acta Neuropathol (Berl)* **108**:413–421.
3. Burger PC, Scheithauer BW, Vogel FS (2002) *Surgical Pathology of the Nervous System and Its Coverings*, 4th edn. Churchill Livingstone: New York.
4. Cankovic M, Mikkelsen T, Rosenblum ML, Zarbo RJ (2007) A simplified laboratory validated assay for MGMT promoter hypermethylation analysis of glioma specimens from formalin-fixed paraffin-embedded tissue. *Lab Invest* **87**:392–397.
5. Cargioli TG, Ugur HC, Ramakrishna N, Chan J, Black PM, Carroll RS (2007) Establishment of an in vivo meningioma model with human telomerase reverse transcriptase. *Neurosurgery* **60**:750–759; discussion 759–760.
6. Dinca EB, Sarkaria JN, Schroeder MA, Carlson BL, Voicu R, Berger MS, James CD (2007) Bioluminescence monitoring of intracranial gliolastoma xenograft response to primary and salvage temozolomide therapy. *J Neurosurg* **107**:610–616.
7. Esteller M, Hamilton SR, Burger PC, Baylin SB, Herman JG (1999) Inactivation of the DNA repair gene O6-methylguanine-DNA methyltransferase by promoter hypermethylation is a common event in primary human neoplasia. *Cancer Res* **59**:793–797.
8. Friedman HS, Kerby T, Calvert H (2000) Temozolomide and treatment of malignant glioma. *Clin Cancer Res* **6**:2585–2597.
9. Hasegawa K, Pham L, O'Connor MK, Federspiel MJ, Russell SJ, Peng KW (2006) Dual therapy of ovarian cancer using measles viruses expressing carcinoembryonic antigen and sodium iodide symporter. *Clin Cancer Res* **12**:1868–1875.
10. Hegi ME, Diserens AC, Gorlia T, Hamou MF, de Tribolet N, Weller M *et al* (2005) MGMT gene silencing and benefit from temozolomide in glioblastoma. *N Engl J Med* **352**:997–1003.
11. Kalamarides M, Niwa-Kawakita M, Leblois H, Abramowski V, Perricaudet M, Janin A *et al* (2002) Nf2 gene inactivation in arachnoidal cells is rate-limiting for meningioma development in the mouse. *Genes Dev* **16**:1060–1065.
12. Kaplan EL, Meier P (1958) Non-parametric estimation from incomplete observations. *J Am Stat Assoc* **53**:457–481.
13. Lee WH (1990) Characterization of a newly established malignant meningioma cell line of the human brain: IOMM-Lee. *Neurosurgery* **27**:389–395.
14. Lee WH, Tu YC, Liu MY (1988) Primary intraosseous malignant meningioma of the skull: case report. *Neurosurgery* **23**:505–508.
15. Mathiesen T, Lindquist C, Kihlstrom L, Karlsson B (1996) Recurrence of cranial base meningiomas. *Neurosurgery* **39**: 2–7.
16. McCutcheon IE, Friend KE, Gerdes TM, Zhang BM, Wildrick DM, Fuller GN (2000) Intracranial injection of human meningioma cells in athymic mice: an orthotopic model for meningioma growth. *J Neurosurg* **92**:306–314.
17. Mendenhall WM, Morris CG, Amdur RJ, Foote KD, Friedman WA (2003) Radiotherapy alone or after subtotal resection for benign skull base meningiomas. *Cancer* **98**:1473–1482.
18. Modha A, Gutin PH (2005) Diagnosis and treatment of atypical and anaplastic meningiomas: a review. *Neurosurgery* **57**:538–550.
19. Peto R, Peto J (1972) Asymptotically efficient rank invariant procedures. *J R Stat Soc Ser A Stat Soc* **135**:185–207.
20. Puttmann S, Senner V, Braune S, Hillmann B, Exeler R, Rickert CH, Paulus W (2005) Establishment of a benign meningioma cell line by hTERT-mediated immortalization. *Lab Invest* **85**:1163–1171.
21. Ragel BT, Jensen RL, Gillespie DL, Prescott SM, Couldwell WT (2006) Celecoxib inhibits meningioma tumor growth in a mouse xenograft model. *Cancer* **109**:588–597.
22. Riemenschneider MJ, Perry A, Reifenberger G (2006) Histological classification and molecular genetics of meningiomas. *Lancet Neurol* **5**:1045–1054.
23. Robb VA, Li W, Gutmann DH (2004) Disruption of 14-3-3 binding does not impair Protein 4.1B growth suppression. *Oncogene* **23**:3589–3596.
24. Salhia B, Rutka JT, Lingwood C, Nutikka A, Van Furth WR (2002) The treatment of malignant meningioma with verotoxin. *Neoplasia* **4**:304–311.
25. Schrell UM, Rittig MG, Anders M, Kiesewetter F, Marschalek R, Koch UH, Fahlbusch R (1997) Hydroxyurea for treatment of unresectable and recurrent meningiomas. I. Inhibition of primary human meningioma cells in culture and in meningioma transplants by induction of the apoptotic pathway. *J Neurosurg* **86**:845–852.
26. Surace EI, Lusis E, Haipek CA, Gutmann DH (2004) Functional significance of S6K overexpression in meningioma progression. *Ann Neurol* **56**:295–298.
27. van Furth WR, Laughlin S, Taylor MD, Salhia B, Mainprize T, Henkelman M *et al* (2003) Imaging of murine brain tumors using a 1.5 Tesla clinical MRI system. *Can J Neurol Sci* **30**:326–332.
28. Yoo H, Baia GS, Smith JS, McDermott MW, Bollen AW, Vandenberg SR *et al* (2007) Expression of the hypoxia marker carbonic anhydrase 9 is associated with anaplastic phenotypes in meningiomas. *Clin Cancer Res* **13**:68–75.